Single-cell RNA-seq analysis reveals lung epithelial cell-specific contributions of Tet1 to allergic inflammation

Tao Zhu*[1], Anthony P. Brown*[1], Lucy Cai[1], Gerald Quon[2], Hong Ji[1,3]

*co-authors

[1] California National Primate Research Center; [2] Department of Molecular and Cellular Biology, Genome Center; [3]Department of Anatomy, Physiology and Cell biology, School of Veterinary Medicine, University of California, Davis, CA,

*Corresponding author: Hong Ji, PhD, Department of Anatomy, Physiology and Cell Biology, School of Veterinary Medicine, University of California, Davis, CA, USA; California National Primate Research Center, USA. Phone: 530-754-0679. Email: hgji@ucdavis.edu

Short title: Epithelial cell type specific effects of Tet1 in allergic airway inflammation

Acknowledgements: This work was supported by NIH/NIAID R01AI141569-1A1 (HJ). HJ was also supported by NIH/NIEHS P30ES023513-supported EHSC scholar fund and UC Davis Faculty Startup fund. Funding was also provided by NSF CAREER award 1846559 to GQ.

Abstract Word Count: 250; Text Word Count: 6907.

ABSTRACT

Background Tet1 protects against house dust mite (HDM)-induced lung inflammation in mice and alters the lung methylome and transcriptome. We explored the role of Tet1 in individual lung epithelial cell types in HDM-induced inflammation.

Methods A model of HDM-induced lung inflammation was established in Tet1 knockout and littermate wildtype mice. $EpCAM^+$ lung epithelial cells were isolated. Libraries were generated using the 10X Chromium workflow and sequenced. ScRNA-seq analysis was performed using Cell Ranger, scAlign, and Seurat. Cell types were labeled using known markers. Enriched pathways were identified using Ingenuity Pathway Analysis. Transcription factor (TF) activity was analyzed by DoRothEA. Single-cell trajectory analysis was performed with Monocle to explore Alveolar type 2 (AT2) cell differentiation.

Results AT2 cells were the most abundant among the eight $EpCAM^+$ lung epithelial cell types. HDM challenge increased the percentage of alveolar progenitor cells (AP), broncho alveolar stem cells (BAS), and goblet cells, and decreased the percentage of AT2 and ciliated cells. Bulk and cell-type-specific analysis identified genes subject to Tet1 regulation and linked to augmented lung inflammation, including alarms, detoxification enzymes and oxidative stress response genes, and gene in tissue repair. The transcriptomic regulation was accompanied by alterations in TF activities. Trajectory analysis supports that HDM may enhance the differentiation of AP and BAS cells into AT2 cells, independent of Tet1.

Conclusions Collectively, lung epithelial cells had common and unique transcriptomic signatures of allergic lung inflammation. Tet1 deletion altered transcriptomic networks in various lung epithelial cells, with an overall effect of promoting allergen-induced lung inflammation.

Key words: Allergic lung inflammation; Tet1; Single-cell RNA-seq; Alveolar type 2 (AT2) cells; Single-cell trajectory

INTRODUCTION

Asthma is one of the most common pulmonary disorders with high heterogeneity [1]. Using RNA-sequencing, previous studies have noted significant transcriptomic differences in both asthmatic patients and animals with allergic lung inflammation [2-4]. Recent studies, including ours [2,5-7], have also linked DNA methylation-associated transcriptomic changes to the pathogenesis and progression of asthma. Our previous studies [8-10] suggest that Tet1 (Tet Methylcytosine Dioxygenase 1) contributes to the regulation of DNA methylation and gene expression in asthma. Tet1 belongs to the family of ten-eleven translocation methylcytosine dioxygenases. These demethylases catalyze the hydroxylation of DNA methylcytosine (5mC) into 5-hydroxymethylcytosine (5hmC), 5-formylcytosine (5fC), and 5-carboxycytosine (5caC), interact with histone modifiers and transcription factors, and may contribute to many biological processes and responses to environmental exposures (reviewed in [11]). In a previous study, we found that a cluster of genes, including *Il33*, *Gsto1*, *Aldh1a1*, and *Isg15*, were regulated by Tet1 in HDM-induced lung inflammation in mice and human bronchial epithelial cells (HBECs) [8]. Meanwhile, we found that several signaling pathways, including NRF2-mediated Oxidative Stress Response, Aryl Hydrocarbon Receptor (AhR) Signaling, and Interferon (IFN) signaling pathway, were involved in Tet1 deficiency-enhanced allergic airway inflammation. Nevertheless, given the use of bulk RNA sequencing technologies in these previous studies, critical questions remained on what role Tet1 plays in individual cell types in asthma, and what the most likely cellular origin(s) of specific inflammatory mediators and molecules are. In this study, our primary goal was to explore the role of Tet1 in HDM-induced lung inflammation in individual lung epithelial cells (EpCAM$^+$) from mice using scRNA-seq. The effects of Tet1 loss and HDM challenges were compared in all EpCAM$^+$ cells together and in each individual cell type.

METHODS

Establishment of HDM-induced airway inflammation mouse model and Isolation of CD326$^+$ CD31$^-$

CD45$^-$ (EpCAM$^+$) lung epithelial cells

HDM-induced allergic inflammation was established in both Tet1$^{-/-}$ mice (knockout/KO mice) and their littermate Tet1$^{+/+}$ mice (wildtype/WT mice) as described in a previous study [8] (details in Supplementary methods and Figure S1A). All procedures on animals were approved by the Animal Experimental Ethics Committee of Cincinnati Children's Hospital Medical Center and University of California, Davis. Airway inflammation was assessed by histology. Lobes, about 5mm large, were sectioned in half and collected from each animal. Lobes from animals of the same group were pooled into one sample. Tissues were minced in a collagenase (480U/ml)-dispase (5U/ml)-DNase (80U/ml) digestion solution in DPBS with Ca$^+$ and Mg^{2+} and razor blades. The finely minced tissues were then incubated in 6mL digestion solution at 37°C for 40min with gentle inversion for 30s at 5min intervals. After incubation, samples were washed with a DPBS/1% BSA wash buffer and passed through a 70µm filter strainer. After spinning down cells and removing the supernatant, cells were treated with AKC lysis buffer to remove red blood cells and washed once more to remove dead cells and excess RNA in the buffer. CD45$^+$ cells (immune cells) and CD31$^+$ (endothelial cells) were then depleted using mouse CD45 and CD31 MicroBeads (Miltenyi Biotec) and the remaining cells were counted and incubated with anti-CD326-APC (eBioscience), anti-CD31-PE-cy7 (eBioscience) and anti-CD45-PE (Biolegend). CD326$^+$ CD31$^-$ CD45$^-$ cells were collected on a MoFlo sorter (Beckman Coulter/MoFlo XDP) with >99% purity at the Research Flow Cytometry Core at Cincinnati Children's Hospital Medical Center (Figure S1B).

Single cell library preparation and sequencing

For 10X Genomics single cell RNA sequencing, cells were brought to a concentration of about 1000 cells/µL using the resuspension buffer. 8000 cells were targeted for cDNA preparation and put through the 10X Genomics Chromium Next GEM Single Cell 3’ v3.1 pipeline for library preparation. After cDNA preparation and GEM Generation and clean-up, cDNA was quality checked and quantified on an Agilent Bioanalyzer DNA

High Sensitivity chip at a 1:10 dilution. Successful traces showed a fragment size range of approximately 1000-2000bp. 12 indexing cycles for library was used. The quality of indexed libraries were checked on an Agilent Bioanalyzer DNA High Sensitivity chip at a 1:10 dilution. Successful libraries had fragment size distributions with peaks around 400bp. Libraries were sequenced using 4 Illumina Hiseq lanes (Paired-end 75bp).

Single-cell RNA-sequencing data analysis

We used Cell Ranger v3.1.0 [12] for initial processing of the scRNA-seq data. Specifically, we used Cell Ranger for sample demultiplexing, barcode processing, read alignment to the reference genome, data aggregation, and generating expression matrices. We then imported the data into Seurat v3.1.4 [13] for downstream processing. Cells that had fewer than 700 genes expressed, greater than 10% of reads mapping to the mitochondria, fewer than 20000 unique molecular identifiers, or that expressed Pecam1 (CD31, an endothelial marker [14]) were filtered out. We also used cell cycle markers to identify which part of the cell cycle each cell was in during sampling [15], and subsequently regressed out this variable and the percentage of mitochondrial reads in each cell while normalizing and scaling the data with Seurat. In order to cluster all cell types accurately without biases from the HDM treatment, we used scAlign [16], a program that uses an unsupervised deep learning algorithm to correct for treatment effects that can affect cell clustering. First, the data were separated into two separate files based on treatment, and 3000 variable features were identified in each file separately. Variable features that overlapped were used for downstream clustering. We then performed single cell alignment by performing a bidirectional mapping between cells with different treatments, creating a low-dimensional alignment space where cells grouped together by type rather than by treatment [16]. Our best results (i.e. greatest separation of clusters by type rather than by treatment) were achieved by using the first 50 principal component scores rather than individual gene level data as input to the model. The output from the scAlign model was subsequently used as input for a uniform manifold approximation and projection (UMAP) in Seurat [13] to visualize the cell clusters.

We then used the FindClusters function from Seurat (a shared-nearest-neighbor-based approach) to cluster the cells, using a wide range of resolutions from 0.01 to 2 to identify the best resolution for our dataset. FindClusters is a shared nearest neighbor modularity optimization based clustering algorithm. Our eventual selection was a resolution of 1, yielding 11 initial cell clusters. We then used markers from the single-cell mouse cell atlas [17] and another study on lung epithelial cells [18] to identify cell clusters. For each cluster, we plotted the gene expression levels of the markers from each epithelial cell type in our references, and identified which cell type each cluster represented. We merged some of the original 11 clusters identified by Seurat [13] that expressed similar markers, only merging sister nodes in the cell cluster tree generated by BuildClusterTree from Seurat. After merging similar clusters, we had a total of nine different labeled cell clusters in our dataset. We then used Seurat to calculate cluster means and perform differential expression analyses via the Wilcox Rank Sum Test. For each cell type individually as well as for all cells combined, we performed five differential expression comparisons: 1) WT-HDM vs. WT-Saline, 2) KO-Saline vs. WT-Saline, 3) KO-HDM vs KO-Saline, 4) KO-HDM vs. WT-HDM and 5) KO-HDM vs. WT-Saline. Genes that were differentially expressed had a false discovery rate (FDR) of 0.05 or less, and a fold change of at least 1.2. Genes also had to be expressed in at least ten percent of one of the comparison groups to qualify as differentially expressed. Pathway enrichment analyses for differentially expressed genes from each comparison were performed using IPA (QIAGEN Inc., https://www.qiagenbioinformatics.com/products/ingenuitypathway-analysis).

Transcription factor activity analysis

We used DoRothEA [19-21] to assess the relative transcription factor (TF) activity levels in different cell types and/or treatments. DoRothEA computes activity levels for transcription factors using the expression levels of targets of each TF instead of the expression level of the TF itself. For our analysis, we chose to include only highly confident interactions between TFs and target genes (confidence levels “A”, “B”, or “C”). We used VIPER for statistical analysis of the TF activity levels, as VIPER considers the mode of each TF-target interaction and has been shown to be appropriate for single-cell analysis [21,22]. We compared TF activity between cell types and plotted top 50 by activity level variance. We also compared TF activity within cell types by sample type in AT2 and ciliated cells and plotted top 25.

Single-cell trajectory analysis

In order to assess the differentiation of AP and BAS cells to AT2 cells, we performed single-cell trajectory analysis using Monocle [23]. First, the dataset was subsetted to include only AP, BAS, and AT2 cells using Seurat [13]. Next, cells were ordered based on the progress they had made through the differentiation process via reversed graph embedding using Monocle, then dimensionality reduction was performed using the “DDRTree” reduction method, and cell trajectories were visualized. We also performed trajectory analyses on different subsets of AP, BAS, and AT2 cells to better understand how HDM treatment and Tet1 deletion impacted the differentiation of AP and BAS cells into AT2 cells. We performed cell trajectory analyses on 1) all AP, BAS, and AT2 cells; 2) only wildtype AP, BAS, and AT2 cells; 3) only AP, BAS, and AT2 cells that had Tet1 knocked out; 4) only saline treated AP, BAS, and AT2 cells; 5) only HDM treated AP, BAS, and AT2 cells. For each of these comparisons, we also performed branched expression analysis modeling within Monocle to identify genes that were differentially expressed along the trajectory at branch points that roughly separated AP, BAS, and AT2 cells. However, this was not possible in the saline cell only group, as there were no branch points that clearly separated these different groups of cells. We then used Monocle to make heatmaps visualizing the expression patterns of genes that showed a significant change in expression along these trajectories ($q < 1 \times 10^{-4}$).

RESULTS

Single-cell analysis identified nine cell types in the EpCAM$^+$ CD45$^-$ CD31$^-$ cells from mouse lungs.

In order to understand the contribution of Tet1 expression in lung epithelium to allergic inflammation, we isolated EpCAM$^+$ CD45$^-$ CD31$^-$ (EpCAM$^+$) lung epithelial cells from animals in an established HDM-induced allergic airway inflammation model [8] and characterized them using single-cell RNAseq (overall study design in Figure 1A, treatment protocol and isolation strategy in Figure S1A and S1B). To demonstrate the successful establishment of allergen-induced lung inflammation, pathological alterations were observed. Consistent with our previous observations [8], airway inflammatory cells infiltration, goblet cell proliferation, smooth muscle hypertrophy, and airway basement membrane thickening were observed in HDM-challenged WT (WT-HDM) mice included in the single-cell analysis (Figure S1C and S1D). Slightly more inflammatory cells infiltration, goblet cell proliferation, and airway mucus secretion were observed in HDM-challenged KO mice (KO-HDM) included in this scRNA-seq analysis. No pathological changes were observed in both WT-Saline and KO-Saline mice.

Among the 25,437 cells we sequenced that passed our quality filters, we identified nine distinct cell types (Figure 1B/1C) based on established marker expression patterns (Figure 1D, Table S1). We identified AT2 cells, alveolar progenitor (AP), broncho alveolar stem (BAS), ciliated cells, stromal cell, club cells, goblet, neuroendocrine cells, and AT1 cells, in order of abundance (Figure 2 and Table S2). AT2 cells were by far the most abundant (17,729 out of 23,437 were AT2 cells). On average, we observed a 24.9% increase in AP cells (2.0% ± 0.6%→26.9% ± 2.1%) and 11.1% increase in BAS cells (1.0% ± 0.2%→12.1% ± 3.0%) following HDM challenges, while the percentage of AT2 cells (85.3% ± 1.4%→56.1% ± 0.04%) and ciliated cells (4.6% ± 1.5%→1.5% ± 0.7%) decreased following HDM challenges (Figure 2 and Table S2). A small increase in the percentage of goblet cells following HDM challenges was also observed, consistent with goblet cell metaplasia in histological studies (Figure S1C and S1D). Although we expect cell loss during single-cell suspension preparation and cell sorting, these results suggest dynamic changes of AP, BAS, AT2, ciliated and goblet cells in HDM-induced lung inflammation. Additionally, since stromal cells are not epithelial cells, we will not discuss DEGs in stromal cells further in this study.

Exposure to HDM led to cell type-specific changes in the EpCAM$^+$ lung epithelial cells.

We identified 830 differentially expressed genes (DEGs) between all WT-HDM and WT-Sal cells in analysis of all EpCAM$^+$ cells (hereafter referred to as bulk cell analysis), regardless of cell type (Table 1, Table S3 and Figure S2). Of the 830 DEGs, 560 were upregulated and 270 were downregulated in WT-HDM. As predicted, several pathways were significantly activated or inhibited, including Oxidative Phosphorylation (activation z-score=7.353), Sirtuin Signaling Pathway (z-score=-2.897) and Xenobiotic Metabolism AHR Signaling Pathway (z-score=-2.111) (Table S4). We further identified DEGs within each of the 8 cell types in the WT-HDM vs WT-Saline comparison. In total, we found 1773 DEGs, greater than the number of DEGs identified in the bulk cell analysis (Table 1). All cell types except AT1 cells had some differential expression associated with HDM treatment. Of these 1773 DEGs, 616 were unique to one cell type (Figure 3). AT2 cells had the most differentially expressed genes associated with HDM treatment (n=732), followed by AP (n=431) (Table 1, Figure 3A, Table S5, and Figure S2). Among the 732 DEGs identified in AT2 cells, 476 were upregulated (including *Il33*, *Gstt1*, *Isg15*, *Iftm3*, and *Cxcl15*) and 256 were downregulated (e.g., *Gstm1*) in WT-HDM compared to WT-Sal. Many genes, including *Il33* [24], *Cxcl5* [25], *Cxcl15* [26], *Ccl20* [27], *Cxcl3* [28], *Cxcl1* [29], *C3* [30], that have been linked to asthma pathogenesis showed cell type-specific response to HDM (Figure 4F-4H, Tables S5 and S6). Subsequently, pathway analysis identified a total of 120 significantly enriched pathways (Table S7). Besides 98 pathways shared with in bulk cell analysis, 22 pathways are unique to AT2 cells, including Ferroptosis Signaling Pathway, Chemokine Signaling, LPS-stimulated MAPK Signaling, etc. Additionally, 79 IPA pathways were enriched in the 318 unique DEGs in AT2 cells.

Chronic airway inflammation induced by inhaled allergens plays a critical role in the pathophysiology of asthma. Ciliated cells are one major cell type that contributes to mucociliary clearance of pathogens, and therefore is subject to injury and chronic inflammation. Inflammatory mediators, such as Th2 cytokines (IL-4, IL-5, and IL-13), can directly cause inflammation and injury in ciliated cells in asthma [31,32]. Moreover, injured ciliated cells will release more inflammatory mediators, such as TSLP and IL-33, leading to more airway inflammation and obstruction [33,34]. A total of 210 DEGs were found in ciliated cells in the WT-Sal vs WT-HDM comparison, with 104 of these genes being unique to ciliated cells (Table 1, Figure 3A, Figure S2, Tables S5 and S6). Compared with WT-Sal, 155 DEGs were upregulated (e.g., *Il33* and *Ifitm3*) and 55 DEGs were downregulated (e.g., *Gstp1*, *Gstm1* and *Gpx2*) in WT-HDM ciliated cells (examples shown in Figure 4K-4N). Other DEGs from this comparison, such as *Fos* [35], *Jun* [36], *Hes1* [37], *Cd14* [38] and *C3* [30], have been associated with asthma pathogenesis. Subsequently, 96 significantly enriched pathways in these DEGs were identified (Table S8). NRF2-mediated Oxidative Stress Response was predicted to be inhibited (z-score=-2.333). Furthermore, 18 IPA pathways were enriched in the 104 unique DEGs in ciliated cells (Table S8). Among them, some pathways, such as NRF2-mediated Oxidative Stress Response (*Dnajc5*, *Gpx2*, *Gstm6*, and *Maff*) and Antigen Presentation Pathway (*Cd74* and *Hla-e*) [39], have been linked to asthma. Collectively, these results suggest that different types of EpCAM$^+$ lung epithelial cells contribute to the allergic responses to HDM and pathogenesis of asthma, with common features as well as unique functions.

Tet1 knockout led to cell-specific changes in baseline EpCAM$^+$ lung epithelial cells.

In the bulk analysis of EpCAM$^+$ cells comparing KO-Sal and WT-Sal, 98 genes were differentially expressed (Table 1, Figure S2, and Table S3). There were 27 significantly enriched pathways associated with these DEGs (Table S4), including several stress-related pathways (Protein Ubiquitination Pathway/Unfolded protein response/eNOS Signaling/NRF2-mediated Oxidative Stress Response/Glutathione Redox Reactions I), and pro-inflammatory pathways (Interferon Signaling/IL-6 Signaling/ IL-12 Signaling and Production in Macrophages). Furthermore, we identified DEGs in each cell type (Table 1 and Table S5). A total of 70 DEGs were found in AT2 cells, including 48 DEGs unique to AT2 cells (e.g., *Il33*, *Malat1* and *S100a6*) (Table S5 and Figures 3B, example plots shown in Figures 4, 5 and Figure S3). Compared with WT-Sal, 42 DEGs were upregulated (e.g., *IL33*) and 28 DEGs were downregulated (e.g., *Lrg1* and *Areg*) in KO-Sal. There were 45 significantly enriched IPA pathways (Table S7), including 17 found in bulk cell analysis and 28 unique ones to AT2 cells (e.g., AhR Signaling/Xenobiotic Metabolism AHR Signaling Pathway). Several genes, *Areg* [40] and *Bpifa1* [41], *Hspa8* [42] and *Lgals3* [43] (also DEGs in ciliated cells), have previously been linked to asthma.

Additionally, 41 Tet1 loss-induced DEGs were found in ciliated cells (Table 1, Table S5 and Figure 3B). Compared with WT-Sal, 24 DEGs were upregulated and 17 DEGs were downregulated in KO-Sal. Several asthma-related genes were identified: detoxification enzymes (*Cyp2a5* [44], *Gsto1* [45], *Gstp1* [46], *Gstm1* [47], and *Aldh1a1* [45]) were downregulated while *Hmgb1* (alarmin) [48 49] was upregulated (Figure 4L-4O, Tables S5 and S6). Consistent with our observations following HDM treatment, the downregulation of the detoxification enzymes by Tet1 (*Gstp1, Gstm1*, and *Gpx2*) were only found in ciliated cells (Figure 4L-4N and Table S6). *Hmgb1* was also found to be upregulated in AT2 cells. 49 significantly enriched pathways were identified in ciliated cells (Table S8), which revealed the significant inactivation of Xenobiotic Metabolism AHR Signaling Pathway (z-score= -2.449) and enrichment of several other stress response pathways.

In summary, our single-cell analysis comparing WT-Saline and KO-Saline found that loss of Tet1 in saline-treated mice 1) increased the expression of alarmins, particularly *Il33* (AT2 cells) and *Hmgb1* (AT2 and ciliated cells), that promote type 2 inflammation, 2) upregulated genes that promote proliferation and migration of airway smooth muscle cells and tissue remodeling [*Malat1* (AT2 cells) and *Pfn1* (6 cell types)], and 3) reduced the expression of detoxification enzymes (*Gpx2*, *Gstm1*, *Gsto1*, and *Gstp1*) in AhR Signaling in ciliated cells. Together, this gene dysregulation by Tet1 loss may result in a pro-inflammatory state in AT2 and ciliated cells.

Tet1 knockout and HDM exposure induced overlapping cell type-specific changes in the EpCAM+ lung epithelial cells.

To further explore the effects of Tet1 knockout in HDM-induced lung inflammation, we searched for overlapping genes among the WT-HDM vs WT-Sal, KO-Sal vs WT-Sal, and KO-HDM vs WT-Sal comparisons. 48 overlapping DEGs were identified, including 36 with changes in the same directions (14 upregulated and 22 downregulated) in bulk cell analyses (Table 1 and Table S9). Thirteen genes were linked to different aspects of asthma, including 8 upregulated genes (*Il33, Hmgb1*, *Ager*, *Chia1*, *Ifitm3, Igfbp7*, *Pfn1*, *Retnla*) and 5 downregulated genes (*Atf3*, *Btg2*, *Klf6*, *Neat1*, and *Sec14l3*) (Figures 4A/4B and S3-B1-B12). Eight mitochondrially encoded genes were also among the 36 overlapping DEGs, but their role in asthma is not clear. Next, overlapping DEGs within each cell type were explored. In AT2 cells, 39 genes were found differentially expressed in all 3 different comparisons (WT-HDM vs WT-Sal, KO-Sal vs WT-Sal, and KO-HDM vs WT-Sal) in AT2 cells (Table S9). 30 genes have changes in the same direction (12 upregulated and 18 downregulated), 27 of which were also found in bulk cell analysis. Meanwhile, there were 5 genes that were consistently downregulated in ciliated cells among the three aforementioned comparisons (Table S9), including asthma-associated genes, *Gstp1*, *Gstm1*, and *Gpx2* (Figure 4L-4N). Additionally, we found that 2 genes (*Dmkn* and *Chia1*) in AP cells and 1 gene (*Nnat*) in BAS cells were consistently changed in these 3 comparisons. IPA analysis revealed several significant diseases and functions affected by these overlapping genes, including inflammation of organ in EpCAM^{+} cells and AT2 cells (Figure 6A/6B), Cell proliferation of fibroblast in AT2 cells (Figure 6C) and Synthesis of reactive oxygen species in ciliated cells (Figure 6D).

The finding that several genes had consistent gene expression changes of direction in 3 comparisons indicates that these changes were mediated similarly by Tet1 knockout, HDM exposure, and Tet1-knockout plus HDM, which suggests that this cluster of genes contributed substantially to Tet1 knockout-enhanced HDM-induced lung inflammation in mice. Furthermore, our data suggest that the effects of Tet1 knockout in allergen-induced lung inflammation were cell-type dependent, and that individual cell types play specific and sometimes separate roles in the pathogenesis of asthma.

Tet1 dysregulates the single-cell transcriptomic signature of HDM-induced lung inflammation in mice.

In order to further understand the effects of Tet1 loss in presence of HDM, we looked into the 72 genes that were differentially expressed in KO-HDM compared with WT-HDM in all EpCAM$^+$ cells (Figure S2 and Table S3). 34 genes were upregulated [e.g., *Areg* (Fig 5A), *Malat1* (Fig 5B), *Sox9* (Fig 5C), and *S100a1* (Fig 5D)] and 38 downregulated [e.g., *Lrg1* (Fig 5E) *and Ifitm3* (Fig S3-B3), *Cxcl1*, and *Rnase4*] (Table S6). Among the 72 DEGs, 29 significantly enriched pathways were identified (Table S4), which included several stress response pathways (e.g., Protein Ubiquitination Pathway/ Unfolded protein response/ Endoplasmic Reticulum Stress Pathway/ NRF2-mediated Oxidative Stress Response) and proinflammatory pathways (e.g., Interferon signaling pathway/ Antigen Presentation Pathway/ Natural Killer Cell Signaling). This is consistent with our previous observations in bulk RNA-seq from total lungs in mice challenged using the same exposure protocol [8]. Surprisingly, several genes upregulated by HDM challenges, such as *Cxcl5* (Fig 4C)/*Isg15*/*Ifitm3* (Fig S3-B3)/*Lrg1* (Fig 5E), showed reduced expression in KO-HDM compared to WT-HDM (Table S6). In contrast, other genes involved in tissue injury/repair and remodeling, such as *Areg* (Fig 5A) [50,51], *Malat1* (Fig 5B) [52,53], *S100a1* (Fig 5D) [54,55], *Mt1/2* (Fig 5F/5G) [56,57], *Scgb1a1* (Fig 5H) [58,59] and *Clu* [60,61], were upregulated in KO-HDM compared to WT-HDM, even though some of these genes (e.g., *Areg*) were downregulated in KO-Sal mice compared to WT-Sal mice.

We then compared KO-HDM with WT-HDM in each cell type. Interestingly, of the 195 DEGs identified across all cell types, 194 were found in AP cells, AT2 cells, and BAS cells (Table 1 and Figure 3D), and 32 DEGs were shared among all three of these cell types. All 32 of these common DEGs changed in the same direction: 16 were upregulated (e.g., *Areg*, *Malat1*, *Mt1*/*2*, and *Scgb1a1*) and 16 were downregulated (e.g., *Cxcl5*, *Cxcl1*, *Lrg1*, *Pfn1*, and *Rnase4*) in these 3 cell types following Tet1 deletion (Figure 5I/5J/5L, Tables S5 and S6). In AT2 cells specifically, 38 DEGs were upregulated while 40 DEGs were down-regulated in KO-HDM compared to WT-HDM. Among these 78 genes, several genes have previously been linked to asthma, including *H3f3b* (Fig 5M) [42], *Cd200 (*Fig 5N*)* [62], *Phlda1* (Fig 5O*)* [63], and *Acot7* [64] (Figure 5 and Table S6). Further, we identified 32 significantly enriched pathways in the DEGs (p-value<0.05) from AT2 cells (Table

S7), including stress response pathways [Unfolded protein response/Endoplasmic Reticulum Stress Pathway/ Protein Ubiquitination Pathway/NRF2-mediated Oxidative Stress Response, Peroxidation of lipid (Figure 6E)], in which most genes showed downregulation in KO-HDM. In particular, Unfolded protein response was predicted to be inhibited (z=-2.236). Similar to the analysis in all cells, several genes encoding chemokines and cytokines (e.g., *Ccl20*, *Cxcl6*, *Cxcl5*, *Cxcl3*, and *Cxcl1*) showed reduced expression in KO-HDM (Table S6). Interestingly, *Sftpc* was significantly downregulated in AP and BAS cells in KO-HDM. This gene was downregulated in AT2 cells in KO-HDM compared to WT-HDM (FDR=6.75E-20, fold of change=1.09), and in KO-Saline compared to WT-Saline (FDR=4.01E-49, fold of change=1.05) but did not meet out our fold of change cutoff. Surfactant protein C (SP-C) encoded by this gene enhances the ability of surfactant phospholipids to decrease alveolar surface tension [65] and the deficiency of SP-C promotes alveolar instability, associated with lung inflammation and injury [66] [67]. In summary, our data suggest that following HDM challenges, loss of Tet1 led to downregulation of genes in stress response pathways and surfactant proteins, which may lead to significant cell apoptosis and tissue injury (suggested by upregulation of genes involved in tissue damage and repair) and result in additional lung inflammation and remodeling.

Tet1 knockout and HDM exposure induced cell type-specific changes in transcription factor (TF) activity in the EpCAM$^+$ lung epithelial cells.

As Tet1 may regulate gene expression through interacting with TFs, TF activity in individual cell types was explored using DoRothEA [19-21]. Consistent with previous findings [68-70], we observed cell type-specific TF activity, consistent with their cell-type specific regulation of gene expression programs (Figure 7A). For example, *E2f1-4* and *Tfdp1* (both promotes expression of cell-cycle related network [68]) were highly activated in BAS compared to all other cell types, while the activities of *Rest* (a repressor of neuronal genes in non-neuronal cells [71]) and *Rreb1* were lowest in Neuroendocrine cells. Additionally, there was relatively high activity of *Rfx1* (promotes ciliogenesis [72,73]) in ciliated cells. Meanwhile, because AT2 cells were the most abundant cell type, there were generally only small changes in TFs activity compared to the average level. However, a group of TFs, including *Foxa1*, *Sox10*, and *Runx2*, showed relatively high activity levels in AT2 cells, and these TFs are essential in conducting airway and alveolar epithelium development and repair [74-76]. Subsequently, we found that TF activity levels were altered by HDM and Tet1 loss among individual cell types, such as AT2 cells (Figure 7B-7E) and ciliated cells (Figure 7F-7H). For example, regardless of Tet1 status, *Foxa1* (also decreased in expression in HDM samples in AT2 cells, Table S5) and *Hnf1a* activities were reduced by HDM in AT2 cells (Figure 7B), while the activities of *Rest, Rreb1*, and *Nr2c2* were increased by HDM in both AT2 cells and ciliated cells (Figure 7B and 7F). Meanwhile, *Smad3*, *Smad4*, and *Sp3* activities were decreased by HDM in ciliated cells (Figure 7F). When specifically looking for effects of Tet1, we found that the activities of *Myc, Rest* and *Rreb1* were consistently reduced when Tet1 was lost in AT2 cells regardless of HDM status (Figure 7C). Hif1α, whose expression is regulated by Tet1 [77] and may also regulate Tet1 expression [78], showed reduced activity in KO-Saline (Figure 7D). Increased *Foxa1* activity was only observed in KO-HDM compared to WT-HDM (Figure 7E). In ciliated cells, however, nearly all effects of Tet1 loss were specific to treatment state (Figure 7F). With saline treatment, activities of *Nfe2l2 (*encoding Nrf2*)*, *Nfe2l1* (encoding Nrf1) and their binding partner Mafk (Figure 7G) [79] were reduced in TET1 KO cells compared to wildtype cells, and these TFs are involved in various stress responses including oxidative stress [80,81] and regulate the expression of ROS-detoxifying enzymes including *Gstp1*, *Gstm1* and *Gpx2* [82]. Meanwhile, TFs involved in the aryl hydrocarbon receptor signaling pathway (AhR) and the TGFβ signaling pathway (Smad3, Smad4) were higher in KO-HDM compared to WT-HDM, even though HDM challenges reduced their activity (Figure 7F/7H). Collectively, our data suggest that TFs respond to HDM challenges and Tet1 loss in a cell type specific manner, which may contribute to the cell-type specific transcriptomic changes and promote lung inflammation.

HDM, not Tet1, promotes the differentiation of AP cells and BAS into AT2 cells.

As observed above, following HDM challenge, AT2 cells were reduced in prevalence while AP and BAS cells were increased in WT-Sal and KO-Sal mice (Figure 2 and Table S2). It is well-established that AT2 cells can differentiate from AP and BAS cells [83,84]. Therefore, single-cell trajectory analysis was performed to explore the roles of HDM and/or Tet1 KO in AT2 cell differentiation (Figure S4/S5). Initially, AT2, AP, and BAS cells from all groups were combined (Figure S4A) and then cell fates were separated at branch point 4 (Figure S4B). Our data support that AT2 cells differentiated from AP and BAS cells. Comparing WT-Sal to WT-HDM and KO-Sal to KO-HDM, HDM challenged cells have a different cell type distribution than saline treated cells (Figure S4C-4H). However, this was not observed in the WT-Sal vs KO-Sal comparison, as no clear branch point was identified to separate cell fates (Figure S4I-4K). Thus, the heatmap of this comparison could not be generated (Figure S5). Deletion of Tet1 had no significant effects on the AP→AT2 or BAS→AT2 trajectories (Figure S4I-4N). Combined with previous evidence in Figure S4 and Table S2, these results suggest that HDM-induced AT2 cells injury promoted the proliferation and differentiation of AP cells and BAS. Meanwhile, Tet1 knockout did not appear to affect the differentiation of AP cells and BAS into AT2 cells.

Discussion

In this study we used scRNA-seq to understand the role of Tet1 in EpCAM$^+$ CD45$^-$ CD31$^-$ lung epithelial cells in HDM-induced lung inflammation at the single-cell level. Eight types of lung epithelial cells and one population of stromal cells were identified. Among them, AT2 cell was the most abundant type. HDM challenge increased the percentage of AP, BAS, and goblet cells, and decreased the percentage of AT2 and ciliated cells. Furthermore, we observed marked cell type-specific transcriptomic alterations in various types of lung epithelial cells following HDM challenge and/or Tet1 deletion in mice. By doing bulk cell and cell type-specific pairwise comparisons, we found upregulation of pro-inflammatory cytokines/alarmins and genes involved in tissue damage/repair and downregulation of genes in multiple oxidative stress response pathways when Tet1 is knockout without or with HDM challenges. These transcriptomic regulations were accompanied by changes in TF activities. Trajectory analysis also supports that HDM may enhance the differentiation of AP and BAS cells into AT2 cells, independent of Tet1. Taken together, our data suggest that different lung epithelial cells played both common and unique roles in allergic lung inflammation. Tet1 deletion altered the networks of genes regulating oxidative stress responses, alarmins, and tissue injury/remodeling in various lung epithelial cells, with an overall effect of promoting allergy-induced lung inflammation and remodeling in mice (proposed model in Figure 8).

The lung is an organ with continuous exposure to environmental challenges, such as allergens and pathogens. The epithelium is the first line of defense for the lung. Lung epithelium (airway epithelium [85] and alveolar epithelium [86,87]) injury and inflammation play critical roles in asthma. Our previous study [8] found that Tet1 deletion enhanced HDM-induced lung inflammation in mice, and that was linked to transcriptomic changes in proinflammatory molecules (*Il33* and *Isg15*) and detoxification enzymes (*Gsto1* and *Aldh1a1*) in total lung RNA. Furthermore, our results showed that 59 pathways, including NRF2-mediated Oxidative Stress Response, AhR Signaling, and the Interferon (IFN) signaling pathway, were significantly altered. However, the role of Tet1 loss in specific lung cell types in allergic airway inflammation and the contribution of individual cell types in HDM-induced whole lung transcriptomic alterations remain unknown. In the present study, we used scRNA-seq to explore transcriptomic changes in different types of lung epithelial cells at the single-level, addressing the aforementioned questions. Two strategies were taken to explore the effects of Tet1 knockout in HDM-induced lung inflammation. First, we searched for DEGs with consistent changes in direction among 3 comparisons (WT-HDM vs WT-Sal, KO-Sal vs WT-Sal, and KO-HDM vs WT-Sal). This set of genes were similarly regulated by HDM and Tet1 KO alone, and HDM plus Tet1 KO in the same directions. Using this strategy, we identified a set of genes [Cluster 1 (45 unique genes after removing duplicates, Table S9), which include alarms (*Il33*, *Hmgb1*, *S100a6*, etc.) in AT2 cells and detoxification enzymes (*Gstp1*, *Gstm2* and *Gpx2*) in ciliated cells. Notably, Tet1 knockout resulted in upregulation of alarms and downregulation of detoxification enzymes (Table S10). Second, we searched for additional changes comparing WT-HDM vs

KO-HDM. This strategy identified another set of genes [Cluster 2 (Figure 5, Tables S3 and S5)], including 72 genes from EpCAM$^+$ cells and 195 genes from AT2, AP and/or BAS cells (103 unique genes after removing duplicates). In this cluster, genes in multiple stress response pathways were downregulated and several genes in tissue repair/remodeling (e.g. *Clu*) and Inflammatory response (e.g. *Cd200*) were significantly upregulated (Figure 6E/6F and Tables S6/S11). Not all genes identified from the bulk cell analysis were found in the analyses in individual cell types, and vice versa. Yet in general, several genes involved in oxidative stress responses, pro-inflammatory responses, alarmins, AhR signaling/detoxification, and tissue damage and repair were differentially expressed in our dataset (Figure 8), and many are known to contribute to asthma based on evidence from animal models and studies in human subjects. Our study, for the first time, not only showed cell-specific expression patterns at baseline and following HDM challenges in the lung epithelium, but also revealed a key role for Tet1 to regulate these genes transcriptionally in a cell-type specific fashion and promote HDM-induced airway inflammation. Future studies focusing on mechanisms through which Tet1 regulates these genes in the lung epithelium would provide more clarity on this regulatory process.

AT2 cells were the most abundant cell type in our dataset (69.7% in total). Although no significant pathological alterations in alveoli were observed in either asthmatic patients or animal models, several studies [86-88] reported that AT2 cells are a major contributor of many inflammatory mediators involved in asthma, In particular, Ravanetti L, *et al.* supported that AT2 cells are one major source of IL-33 in mice with HDM-induced lung inflammation [88]. Our present study supports that HDM may enhance AT2 cells differentiation from AP and BAS cells (Figure S4), which was likely due to HDM-induced AT2 cells injury and death (Figure 2 and Table S2). Our cell type-specific transcriptomic analysis showed that AT2 cells were one of the major sources of a cluster of inflammatory mediators and molecules, especially *Il33* (Fig 4F), *Hmgb1* (Fig 4J), *Ager* (Fig S3-A1), and *Retnla* (Fig S3-A2), in allergen-induced lung inflammation (Table S6). Allergens may induce lung Th2 inflammation through AT2 cell injury which releases alarms such as *Il33* [24] and *Hmgb1* [89], and Tet1 played a critical role in this process by regulating their expression. Additionally, when comparing KO-HDM to WT-

HDM in AT2 cells, we found that genes involved in tissue damage and repair were upregulated, while genes involved in oxidative stress responses were downregulated; most of these genes were also differentially expressed in EpCAM$^+$ cells (Table S6). Downregulation of oxidative stress response pathways, especially unfolded protein response (UPR), may result in apoptosis and cell death [90], and the roles of UPR in oxidative stress response, cytokine production and asthma pathogenesis are emerging [91]. Taken together, our data suggest that while AT2 cells from Tet1 knockout mice at base line (no HDM) have a pro-inflammatory transcriptomic signature such as elevated alarms and reduced detoxification enzymes, HDM challenges may further induce cell damage and death due to elevated oxidative stress and downregulated stress responses.

Ciliated cells are another major cell type within airway epithelium. Ciliated cells are not only essential for mucociliary clearance through their motile cilia coordinated directional movement, but can also sense and respond to allergens, air pollution particles, and pathogens [31,92]. Asthma can cause cilia dysfunction and ultrastructural abnormalities, such as ciliary beat frequency decreasing, dyskinetic and immotile cilia, and disruption of tight junctions, which were closely associated with asthma severity in patients [93]. Meanwhile, multiple studies [34,94] suggest that ciliated cells are a source of cytokines, such as IL-33 and TSLP, in asthma. Our present data indicates that HDM exposure and/or Tet1 deletion significantly altered the transcriptome of ciliated cells. *Gstp1*, *Gstm1*, and *Gpx2* (detoxification enzymes that have been associated with asthma) were all downregulated among WT-HDM vs WT-Sal, KO-Sal vs WT-Sal, and KO-HDM vs WT-Sal comparisons in ciliated cells (Figure 4L-4N). This highlights the unique role of ciliated cells revealed by single-cell analysis and suggest that Tet1 regulates HDM-induced lung inflammation via regulation of AhR signaling/Detoxification and Pro-inflammatory cytokines/Alarmins in ciliated cells (Figures 6D, 7F and 8).

Since we previously observed significant increases in AHR and BALF eosinophils, as well as significant gene expression differences in bulk lung RNA from KO-HDM mice and WT-HDM mice [8], transcriptomic differences between KO-HDM and WT-HDM cells were further explored. We identified 72 DEGs, associated with 29 significantly enriched pathways, between KO-HDM and WT-HDM EpCAM+ cells.

A total of 195 cell-type specific DEGs were found, including 78 DEGs in AT2 cells. However, no overlapping DEGs with consistent directions of changes among all 4 comparisons (WT-HDM vs WT-Sal, KO-Sal vs WT-Sal, KO-HDM vs WT-Sal, and KO-HDM vs WT-HDM) were observed in either all EpCAM$^+$ cells together or in individual cell types. Additionally, we also noted that some DEGs identified from bulk RNA in our previous study, such as *Il13*, *Muc5ac*, *Cyp1a1*, and *Irf7*, were not differentially expressed. We sometimes observed opposite effects of Tet1 knockout following HDM treatment to saline treatment compared to our previous bulk RNA analysis, such as *Scd1* and *Pfn1* in AT2 cells. This inconsistency may be because HDM-induced transcriptomic changes masked the effects of Tet1 knockout in lung epithelial cells. Meanwhile, increased noise in scRNA-seq data, lower power, or the differences in how DEGs were defined in the scRNA-seq dataset compared to our previous bulk RNA-seq studies were also potential reasons for these inconsistencies. Another possible explanation is that only lung epithelial cells (EpCAM$^+$ cells) were analyzed. These DEGs identified from bulk RNA-seq may be present in other lung cell types such as inflammatory cells, airway smooth muscles, and vascular endothelial cells, which will be pursued in future studies. In the case of Muc5ac, we found that it is predominantly expressed in goblet cells and induced by HDM challenges in both WT (p=0.017, fold of change=6.12) and KO mice (p=0.00014, fold of change=3.62). However, due to the small number of goblet cells, none of these comparisons reached FDR significance and no additional significant changes were observed comparing WT-HDM and KO-HDM at p value<0.05. Appreciable transcriptomic changes were also observed in other types of lung epithelial cells, including AP cells, BAS cells, club cells, goblet cells, and neuroendocrine cells, following HDM exposure and Tet1 deletion in mice. However, no transcriptomic differences in AT1 cells were found, likely due to the limited number of AT1 cells we isolated from the lungs (Table 1). Interestingly, we also observed downregulation of several asthma-associated genes (e.g. *Atf3* [95] and *Btg2* [96]) that are normally increased by HDM challenges, which is possibly due to the time-dependent expression pattern of these molecules during acute phase of inflammation and needs further investigation. Nevertheless, our analysis revealed novel changes that were not found in our previous bulk

RNA-seq analysis, which shed light on possible mechanisms of Tet1 in regulating airway inflammation in the presence of HDM.

Additionally, our data also suggest that HDM and/or Tet1 KO in mice lungs led to cell type-specific changes in TF activity levels (Figure 7). For example, *Foxa1* had reduced activity following HDM treatment in AT2 cells, but activity was higher in the KO-HDM samples compared to WT-HDM samples (Figure 7B). Foxa1 has been shown to play a role in maintaining the integrity of epithelial barriers in primary human bronchial epithelial cells [76], so changes in Foxa1 activity could impact the airway epithelium. *Foxa1* also had significantly decreased expression in HDM samples compared to saline samples in AT2 cells (Table S5). Additionally, AhR (aryl hydrocarbon receptor) showed decreased activity levels in HDM samples compared to saline samples in ciliated cells (similar between KO-saline and WT-saline), but KO-HDM samples had higher AhR activity than WT-HDM samples (Figure 7F/7H). In our prior study using human bronchial epithelial cells, we hypothesized that Tet1 protects against HDM-induced allergic inflammation at least partially by regulating the AhR pathway [8]. Data from the current study in ciliated cells supports that AhR activity and the AhR pathway were altered following Tet1 KO and/or HDM treatment (Figure 7F/7H and Figure 8). Meanwhile, the Nrf1/2 activity was lower in KO-Saline mice compared to WT-Saline, which may explain the lower expression of *Gstp1*, *Gstm1* and *Gpx2* in KO-Saline compared to WT-Saline as the Nrf2-mediated pathway is an alternative to the AhR pathway that regulates the expression of antioxidant enzymes [82]. Smad3, Smad4, Fos, and Atf2 activity levels were all altered by HDM treatment and/or Tet1 KO in AT2 and ciliated cells (Figure 7B/7F/7H). *Fos* also had significantly decreased expression following HDM treatment in AT2 and ciliated cells (Table S5), but not following Tet1 KO. These transcription factors are all part of the AP-1 signaling pathway, which has been previously associated with regulation of asthmatic inflammation [97,98]. These activity levels for the transcription factors were estimated using gene expression profiles of their targets, not based on the direct expression of the transcription factor itself. Even if the direct expression of a transcription factor was not significantly altered, it is still possible that the way that the transcription factors are regulating gene expression could be altered by Tet1 KO or HDM treatment, especially considering that Tet1 is known to directly interact with transcription factors [99,100]. Taken together, these results indicate that Tet1 plays an important role in regulating TF activity that directly impacts allergen-induced lung inflammation.

Collectively, our results revealed possible mechanisms underlying the protective role of Tet1 in HDM-induced lung inflammation at the single-cell level. Different epithelial cells played common and unique roles in allergic lung inflammation. The major cellular contributors of multiple asthma-associated inflammatory mediators, such as *Il33*, *Hmgb1*, *Retnla*, and *Ager* were identified, and a cluster of novel allergy-associated molecules, such as *Chia1*, *Nnat*, and *Nr4a1* were found in different lung epithelial cells. Future studies should attempt to elucidate the role of these novel targets in asthma. Our results suggest that AT2 cell are essential for Th2 inflammation through stress responses, alarms, tissue injury and repair in allergen-induced lung inflammation, and that these genes are regulated by Tet1. In ciliated cells, Tet1 promotes the Xenobiotic Metabolism AhR signaling pathway, especially the detoxification enzymes, to protect from allergen-induced lung inflammation. Overall, these novel findings support that Tet1 is a potential therapeutic target of asthma.

Authors’ Contributions

HJ conceived the study. TZ drafted the manuscript with the help of APB and HJ. TZ established and characterized the mouse model with the help of LC. APB performed scRNA-seq data processing and analysis. LC performed sample processing and assisted in library preparation. GQ assisted in scRNA-seq data processing and provided input in cell clustering. All authors have approved the final version of this manuscript. Part of this study has been published as an abstract (https://doi.org/10.1164/ajrccm-conference.2019.199.1_MeetingAbstracts.A6041 and https://doi.org/10.1164/ajrccm-conference.2020.201.1_MeetingAbstracts.A7402).

Competing interests

The authors declare no competing interest.

Tables

Table 1. Number of Differential expression genes (DEGs) of EpCAM$^+$ cells

Comparisons	WT-HDM vs WT-Sal	KO-Sal vs WT-Sal	KO-HDM vs WT-Sal	Overlap of three comparisons (Same direction)	KO-HDM vs WT-HDM
Bulk cell RNA-seq					
EpCAM+ cells	830	98	817	48 (36)	72
ScRNA-seq					
AT1 cells	0	0	1	0	0
AT2 cells	732	70	745	39 (30)	78
Alveolar progenitor cells	431	18	445	4 (2)	65
Broncho alveolar stem cells	172	4	154	1(1)	51
Ciliated cells	210	41	200	5 (5)	0
Stromal cells	72	19	54	0	1
Club cells	55	5	88	0	0
Goblet cells	13	0	0	0	0
Neuroendocrine cells	88	3	16	0	0
Total	1773	160	1703	49 (45)	195

Figure legend

Figure 1. Single-cell RNA sequencing clustering analysis identifies 9 cell types in $EpCAM^+$ $CD45^-$ $CD31^-$ lung cells.

(A) Schematic overview of the study workflow.

(B) UMAP visualization of clustering revealed 9 cell populations. Population identities were determined based on marker gene expression.

(C) UMAP visualization of $EpCAM^+$ $CD45^-$ $CD31^-$ lung cells in Tet1 KO mice and WT mice with and without HDM challenge.

(D) Heatmap of top 4 markers in 9 cell clusters.

Figure 2. The abundance and percentage of each cell type.

(A) Abundance of each cell type at each condition; (B) Percentage of each cell type at each condition

Figure 3. UpSet plots for overlapped DEGs among 8 individual cells types. (A) WT-Sal vs WT-HDM; (B) WT-Sal vs KO-Sal; (C) KO-HDM vs WT-Sal; (D) KO-HDM vs WT-HDM. Dots below vertical bars represent overlapped DEGs among different cell types. Horizontal bars represent the total number of DEGs in each cell types.

Figure 4. Cell-type specific changes resulting from HDM challenges and/or Tet1 deficiency. (A-E) All $EpCAM^+$ cells; (F-J) AT2 cells; (K-O) Ciliated cells.

Figure 5. Tet1 loss promotes HDM-induced lung inflammation by upregulation of proinflammatory responses and tissue damage and repair, and downregulation of genes involved in oxidative stress. (A-H) All $EpCAM^+$ cells; (I-P) AT2 cells.

Figure 6. Diseases and Function analysis in EpCAM$^+$, AT2 and ciliated cells via IPA. (A-D) DEGs with consistent direction changes among 3 comparisons (WT-HDM vs WT-Sal, KO-Sal vs WT-Sal, and KO-HDM vs WT-Sal). (A) Inflammation of organ in EpCAM$^+$ cells. (B) Inflammation of organ in AT2 cells. (C) Cell viability of fibroblast in AT2 cells. (D) Synthesis of reactive oxygen species in ciliated cells. (E) Peroxidation of lipid and (F) Cell viability of fibroblast cell lines in DEGs in KO-HDM vs WT-HDM in AT2 cells.

Figure 7. Heatmaps of transcription factor (TFs) activities analyzed using DoRothEA. (A) Top 50 most variable TFs by gene activity across eight individual cell types. (B) Top 25 TFs across all AT2 cells. (C) TFs that were in the top 25 in both the KO-HDM vs WT-HDM and KO-Saline vs WT-Saline comparisons in AT2 cells. (D) Top 25 TFs in the KO-Saline vs WT-Saline comparison that were not in the top 25 for KO-HDM vs WT-HDM in AT2 cells. (E) Top 25 TFs in the KO-HDM vs WT-HDM comparison that were not in the top 25 for KO-Saline vs WT-Saline in AT2 cells. (F) Top 25 most variable TFs in ciliated cells. (G) Top 25 most variable TFs in ciliated cells in KO-Saline vs. WT-Saline. (H) Top 25 most variable TFs in ciliated cells in KO-HDM vs. WT-HDM.

Figure 8. Proposed model. Tet1 deletion promotes allergy-induced lung inflammation and remodeling in mice, involving down-regulation of genes in AhR signaling/detoxification (ciliated cells) and oxidative stress responses (AT2 cells), and up-regulation of genes in pro-inflammatory cytokines/alarmins (AT2 and ciliated cells) and tissue damage and repair (AT2 cells).

References

1. Scherzer R, Grayson MH. Heterogeneity and the origins of asthma. *Ann Allergy Asthma Immunol.* 2018;121(4):400-405.
2. Xu CJ, Soderhall C, Bustamante M, et al. DNA methylation in childhood asthma: an epigenome-wide meta-analysis. *Lancet Respir Med.* 2018;6(5):379-388.
3. Lee Y, Hwang YH, Kim KJ, et al. Proteomic and transcriptomic analysis of lung tissue in OVA-challenged mice. *Arch Pharm Res.* 2018;41(1):87-100.
4. Cui J, Lv Z, Teng F, et al. RNA-Seq Expression Analysis of Chronic Asthmatic Mice with Bu-Shen-Yi-Qi Formula Treatment and Prediction of Regulated Gene Targets of Anti-Airway Remodeling. *Evid Based Complement Alternat Med.* 2021;2021:3524571.
5. Zhu T, Zhang X, Chen X, et al. Nasal DNA methylation differentiates severe from non-severe asthma in African-American children. *Allergy.* 2021;76(6):1836-1845.
6. Forno E, Wang T, Qi C, et al. DNA methylation in nasal epithelium, atopy, and atopic asthma in children: a genome-wide study. *Lancet Respir Med.* 2019;7(4):336-346.
7. Qi C, Jiang Y, Yang IV, et al. Nasal DNA methylation profiling of asthma and rhinitis. *The Journal of allergy and clinical immunology.* 2020;145(6):1655-1663.
8. Burleson JD, Siniard D, Yadagiri VK, et al. TET1 contributes to allergic airway inflammation and regulates interferon and aryl hydrocarbon receptor signaling pathways in bronchial epithelial cells. *Sci Rep.* 2019;9(1):7361.
9. Zhang X, Chen X, Weirauch MT, et al. Diesel exhaust and house dust mite allergen lead to common changes in the airway methylome and hydroxymethylome. *Environ Epigenet.* 2018;4(3):dvy020.
10. Somineni HK, Zhang X, Biagini Myers JM, et al. Ten-eleven translocation 1 (TET1) methylation is associated with childhood asthma and traffic-related air pollution. *The Journal of allergy and clinical immunology.* 2016;137(3):797-805 e795.
11. Zhu T, Brown AP, Ji H. The Emerging Role of Ten-Eleven Translocation 1 in Epigenetic Responses to Environmental Exposures. *Epigenet Insights.* 2020;13:2516865720910155.
12. Zheng GXY, Terry JM, Belgrader P, et al. Massively parallel digital transcriptional profiling of single cells. *Nature Communications.* 2017;8(1):14049.
13. Stuart T, Butler A, Hoffman P, et al. Comprehensive Integration of Single-Cell Data. *Cell.* 2019;177(7):1888-1902.e1821.
14. Miettinen M, Lindenmayer AE, Chaubal A. Endothelial cell markers CD31, CD34, and BNH9 antibody to H- and Y-antigens--evaluation of their specificity and sensitivity in the diagnosis of vascular tumors and comparison with von Willebrand factor. *Mod Pathol.* 1994;7(1):82-90.
15. Scialdone A, Natarajan KN, Saraiva LR, et al. Computational assignment of cell-cycle stage from single-cell transcriptome data. *Methods.* 2015;85:54-61.
16. Johansen N, Quon G. scAlign: a tool for alignment, integration, and rare cell identification from scRNA-seq data. *Genome Biology.* 2019;20(1):166.
17. Han X, Wang R, Zhou Y, et al. Mapping the Mouse Cell Atlas by Microwell-Seq. *Cell.* 2018;172(5):1091-1107.e1017.
18. Schilders KAA, Eenjes E, van Riet S, et al. Regeneration of the lung: Lung stem cells and the development of lung mimicking devices. *Respiratory Research.* 2016;17(1):44.
19. Garcia-Alonso L, Holland CH, Ibrahim MM, Turei D, Saez-Rodriguez J. Benchmark and integration of resources for the estimation of human transcription factor activities. *Genome Res.* 2019;29(8):1363-1375.
20. Holland CH, Szalai B, Saez-Rodriguez J. Transfer of regulatory knowledge from human to mouse for functional genomics analysis. *Biochim Biophys Acta Gene Regul Mech.* 2020;1863(6):194431.
21. Holland CH, Tanevski J, Perales-Paton J, et al. Robustness and applicability of transcription factor

and pathway analysis tools on single-cell RNA-seq data. *Genome biology.* 2020;21(1):36.

22. Alvarez MJ, Shen Y, Giorgi FM, et al. Functional characterization of somatic mutations in cancer using network-based inference of protein activity. *Nature genetics.* 2016;48(8):838-847.
23. Trapnell C, Cacchiarelli D, Grimsby J, et al. The dynamics and regulators of cell fate decisions are revealed by pseudotemporal ordering of single cells. *Nature Biotechnology.* 2014;32(4):381-386.
24. Hong H, Liao S, Chen F, Yang Q, Wang DY. Role of IL-25, IL-33, and TSLP in triggering united airway diseases toward type 2 inflammation. *Allergy.* 2020;75(11):2794-2804.
25. Kalchiem-Dekel O, Yao X, Barochia AV, et al. Apolipoprotein E Signals via TLR4 to Induce CXCL5 Secretion by Asthmatic Airway Epithelial Cells. *Am J Respir Cell Mol Biol.* 2020;63(2):185-197.
26. Hong GH, Kwon HS, Lee KY, et al. hMSCs suppress neutrophil-dominant airway inflammation in a murine model of asthma. *Exp Mol Med.* 2017;49(1):e288.
27. Busse PJ, Birmingham JM, Calatroni A, et al. Effect of aging on sputum inflammation and asthma control. *The Journal of allergy and clinical immunology.* 2017;139(6):1808-1818 e1806.
28. Sokulsky LA, Garcia-Netto K, Nguyen TH, et al. A Critical Role for the CXCL3/CXCL5/CXCR2 Neutrophilic Chemotactic Axis in the Regulation of Type 2 Responses in a Model of Rhinoviral-Induced Asthma Exacerbation. *Journal of immunology.* 2020;205(9):2468-2478.
29. Choi Y, Kim YM, Lee HR, et al. Eosinophil extracellular traps activate type 2 innate lymphoid cells through stimulating airway epithelium in severe asthma. *Allergy.* 2020;75(1):95-103.
30. Vedel-Krogh S, Rasmussen KL, Nordestgaard BG, Nielsen SF. Complement C3 and allergic asthma: a cohort study of the general population. *Eur Respir J.* 2021;57(2).
31. Whitsett JA. Airway Epithelial Differentiation and Mucociliary Clearance. *Ann Am Thorac Soc.* 2018;15(Suppl 3):S143-S148.
32. Tanabe T, Rubin BK. Airway Goblet Cells Secrete Pro-Inflammatory Cytokines, Chemokines, and Growth Factors. *Chest.* 2016;149(3):714-720.
33. Hellings PW, Steelant B. Epithelial barriers in allergy and asthma. *The Journal of allergy and clinical immunology.* 2020;145(6):1499-1509.
34. Zhu T, Chen Z, Chen G, et al. Curcumin Attenuates Asthmatic Airway Inflammation and Mucus Hypersecretion Involving a PPARgamma-Dependent NF-kappaB Signaling Pathway In Vivo and In Vitro. *Mediators Inflamm.* 2019;2019:4927430.
35. Patil RH, Naveen Kumar M, Kiran Kumar KM, et al. Dexamethasone inhibits inflammatory response via down regulation of AP-1 transcription factor in human lung epithelial cells. *Gene.* 2018;645:85-94.
36. Guo M, Liu Y, Han X, et al. Tobacco smoking aggravates airway inflammation by upregulating endothelin-2 and activating the c-Jun amino terminal kinase pathway in asthma. *Int Immunopharmacol.* 2019;77:105916.
37. Zeng Z, Wang L, Ma W, et al. Inhibiting the Notch signaling pathway suppresses Th17-associated airway hyperresponsiveness in obese asthmatic mice. *Lab Invest.* 2019;99(12):1784-1794.
38. Feng J, Zhang C, Wang Z, Li Q, Li J, Wang H. Association between CD14 gene promoter polymorphisms with serum total-IgE and eosinophil levels in atopic and non-atopic asthma patients in a Chinese Han population. *The Journal of asthma : official journal of the Association for the Care of Asthma.* 2016;53(2):119-124.
39. Bozza MT, Lintomen L, Kitoko JZ, Paiva CN, Olsen PC. The Role of MIF on Eosinophil Biology and Eosinophilic Inflammation. *Clin Rev Allergy Immunol.* 2020;58(1):15-24.
40. Hachim MY, Elemam NM, Ramakrishnan RK, et al. Blood and Salivary Amphiregulin Levels as Biomarkers for Asthma. *Front Med (Lausanne).* 2020;7:561866.
41. Schaefer N, Li X, Seibold MA, et al. The effect of BPIFA1/SPLUNC1 genetic variation on its expression and function in asthmatic airway epithelium. *JCI Insight.* 2019;4(8).
42. Wong SL, To J, Santos J, et al. Proteomic Analysis of Extracellular HMGB1 Identifies Binding Partners

and Exposes Its Potential Role in Airway Epithelial Cell Homeostasis. *J Proteome Res.* 2018;17(1):33-45.

43. Singhania A, Wallington JC, Smith CG, et al. Multitissue Transcriptomics Delineates the Diversity of Airway T Cell Functions in Asthma. *Am J Respir Cell Mol Biol.* 2018;58(2):261-270.
44. Lkhagvadorj K, Meyer KF, Verweij LP, et al. Prenatal smoke exposure induces persistent Cyp2a5 methylation and increases nicotine metabolism in the liver of neonatal and adult male offspring. *Epigenetics.* 2020;15(12):1370-1385.
45. Yi, Cui J, Wang W, et al. Formononetin Attenuates Airway In fl ammation and Oxidative Stress in Murine Allergic Asthma. *Front Pharmacol.* 2020;11:533841.
46. Lin TJ, Karmaus WJJ, Chen ML, Hsu JC, Wang IJ. Interactions Between Bisphenol A Exposure and GSTP1 Polymorphisms in Childhood Asthma. *Allergy Asthma Immunol Res.* 2018;10(2):172-179.
47. Choi H, Song WM, Wang M, Sram RJ, Zhang B. Benzo[a]pyrene is associated with dysregulated myelo-lymphoid hematopoiesis in asthmatic children. *Environ Int.* 2019;128:218-232.
48. Shang L, Wang L, Shi X, et al. HMGB1 was negatively regulated by HSF1 and mediated the TLR4/MyD88/NF-kappaB signal pathway in asthma. *Life Sci.* 2020;241:117120.
49. Simpson J, Loh Z, Ullah MA, et al. Respiratory Syncytial Virus Infection Promotes Necroptosis and HMGB1 Release by Airway Epithelial Cells. *American journal of respiratory and critical care medicine.* 2020;201(11):1358-1371.
50. Todd JL, Kelly FL, Nagler A, et al. Amphiregulin contributes to airway remodeling in chronic allograft dysfunction after lung transplantation. *Am J Transplant.* 2020;20(3):825-833.
51. Nordgren TM, Heires AJ, Bailey KL, et al. Docosahexaenoic acid enhances amphiregulin-mediated bronchial epithelial cell repair processes following organic dust exposure. *American journal of physiology Lung cellular and molecular physiology.* 2018;314(3):L421-L431.
52. Cui H, Banerjee S, Guo S, et al. Long noncoding RNA Malat1 regulates differential activation of macrophages and response to lung injury. *JCI Insight.* 2019;4(4).
53. Lin L, Li Q, Hao W, Zhang Y, Zhao L, Han W. Upregulation of LncRNA Malat1 Induced Proliferation and Migration of Airway Smooth Muscle Cells via miR-150-eIF4E/Akt Signaling. *Front Physiol.* 2019;10:1337.
54. Rohde D, Schon C, Boerries M, et al. S100A1 is released from ischemic cardiomyocytes and signals myocardial damage via Toll-like receptor 4. *EMBO Mol Med.* 2014;6(6):778-794.
55. Brinks H, Rohde D, Voelkers M, et al. S100A1 genetically targeted therapy reverses dysfunction of human failing cardiomyocytes. *J Am Coll Cardiol.* 2011;58(9):966-973.
56. Ma WY, Song RJ, Xu BB, et al. Melatonin promotes cardiomyocyte proliferation and heart repair in mice with myocardial infarction via miR-143-3p/Yap/Ctnnd1 signaling pathway. *Acta Pharmacol Sin.* 2021;42(6):921-931.
57. Kim HG, Huang M, Xin Y, et al. The epigenetic regulator SIRT6 protects the liver from alcohol-induced tissue injury by reducing oxidative stress in mice. *J Hepatol.* 2019;71(5):960-969.
58. Rawlins EL, Okubo T, Xue Y, et al. The role of Scgb1a1+ Clara cells in the long-term maintenance and repair of lung airway, but not alveolar, epithelium. *Cell Stem Cell.* 2009;4(6):525-534.
59. Brasier AR. Therapeutic targets for inflammation-mediated airway remodeling in chronic lung disease. *Expert Rev Respir Med.* 2018;12(11):931-939.
60. Habiel DM, Camelo A, Espindola M, et al. Divergent roles for Clusterin in Lung Injury and Repair. *Sci Rep.* 2017;7(1):15444.
61. Hong JY, Kim MN, Kim EG, et al. Clusterin Deficiency Exacerbates Hyperoxia-Induced Acute Lung Injury. *Cells.* 2021;10(4).
62. Lauzon-Joset JF, Langlois A, Lai LJ, et al. Lung CD200 Receptor Activation Abrogates Airway Hyperresponsiveness in Experimental Asthma. *Am J Respir Cell Mol Biol.* 2015;53(2):276-284.

63. Baos S, Calzada D, Cremades-Jimeno L, et al. Discriminatory Molecular Biomarkers of Allergic and Nonallergic Asthma and Its Severity. *Front Immunol.* 2019;10:1051.

64. Cardenas A, Sordillo JE, Rifas-Shiman SL, et al. The nasal methylome as a biomarker of asthma and airway inflammation in children. *Nat Commun.* 2019;10(1):3095.

65. Hong D, Qi Y, Liu J, Wang H, Wang L, Qian L. A novel surfactant protein C mutation resulting in aberrant protein processing and altered subcellular localization causes infantile interstitial lung disease. *Pediatric research.* 2017;81(6):891-897.

66. Erpenbeck VJ, Schmidt R, Gunther A, Krug N, Hohlfeld JM. Surfactant protein levels in bronchoalveolar lavage after segmental allergen challenge in patients with asthma. *Allergy.* 2006;61(5):598-604.

67. Jin H, Ciechanowicz AK, Kaplan AR, et al. Surfactant protein C dampens inflammation by decreasing JAK/STAT activation during lung repair. *American journal of physiology Lung cellular and molecular physiology.* 2018;314(5):L882-L892.

68. Xu Y, Wang Y, Besnard V, et al. Transcriptional programs controlling perinatal lung maturation. *PloS one.* 2012;7(8):e37046.

69. Little DR, Lynch AM, Yan Y, Akiyama H, Kimura S, Chen J. Differential chromatin binding of the lung lineage transcription factor NKX2-1 resolves opposing murine alveolar cell fates in vivo. *Nat Commun.* 2021;12(1):2509.

70. Zhou P, Gu F, Zhang L, et al. Mapping cell type-specific transcriptional enhancers using high affinity, lineage-specific Ep300 bioChIP-seq. *Elife.* 2017;6.

71. Hohl M, Thiel G. Cell type-specific regulation of RE-1 silencing transcription factor (REST) target genes. *Eur J Neurosci.* 2005;22(9):2216-2230.

72. Lemeille S, Paschaki M, Baas D, et al. Interplay of RFX transcription factors 1, 2 and 3 in motile ciliogenesis. *Nucleic acids research.* 2020;48(16):9019-9036.

73. Patir A, Fraser AM, Barnett MW, et al. The transcriptional signature associated with human motile cilia. *Sci Rep.* 2020;10(1):10814.

74. Besnard V, Wert SE, Kaestner KH, Whitsett JA. Stage-specific regulation of respiratory epithelial cell differentiation by Foxa1. *American journal of physiology Lung cellular and molecular physiology.* 2005;289(5):L750-759.

75. Mummler C, Burgy O, Hermann S, Mutze K, Gunther A, Konigshoff M. Cell-specific expression of runt-related transcription factor 2 contributes to pulmonary fibrosis. *Faseb J.* 2018;32(2):703-716.

76. Paranjapye A, Mutolo MJ, Ebron JS, Leir SH, Harris A. The FOXA1 transcriptional network coordinates key functions of primary human airway epithelial cells. *American journal of physiology Lung cellular and molecular physiology.* 2020;319(1):L126-L136.

77. Zhu J, Wang K, Li T, et al. Hypoxia-induced TET1 facilitates trophoblast cell migration and invasion through HIF1alpha signaling pathway. *Sci Rep.* 2017;7(1):8077.

78. Ali MM, Phillips SA, Mahmoud AM. HIF1alpha/TET1 Pathway Mediates Hypoxia-Induced Adipocytokine Promoter Hypomethylation in Human Adipocytes. *Cells.* 2020;9(1).

79. Johnsen O, Skammelsrud N, Luna L, Nishizawa M, Prydz H, Kolsto AB. Small Maf proteins interact with the human transcription factor TCF11/Nrf1/LCR-F1. *Nucleic acids research.* 1996;24(21):4289-4297.

80. Steffen J, Seeger M, Koch A, Kruger E. Proteasomal degradation is transcriptionally controlled by TCF11 via an ERAD-dependent feedback loop. *Molecular cell.* 2010;40(1):147-158.

81. Radhakrishnan SK, den Besten W, Deshaies RJ. p97-dependent retrotranslocation and proteolytic processing govern formation of active Nrf1 upon proteasome inhibition. *Elife.* 2014;3:e01856.

82. Tonelli C, Chio IIC, Tuveson DA. Transcriptional Regulation by Nrf2. *Antioxidants & redox signaling.* 2018;29(17):1727-1745.

83. Kawakita N, Toba H, Miyoshi K, et al. Bronchioalveolar stem cells derived from mouse-induced pluripotent stem cells promote airway epithelium regeneration. *Stem Cell Res Ther.* 2020;11(1):430.
84. Hogan BL, Barkauskas CE, Chapman HA, et al. Repair and regeneration of the respiratory system: complexity, plasticity, and mechanisms of lung stem cell function. *Cell Stem Cell.* 2014;15(2):123-138.
85. Gon Y, Hashimoto S. Role of airway epithelial barrier dysfunction in pathogenesis of asthma. *Allergol Int.* 2018;67(1):12-17.
86. Huang J, Yue H, Jiang T, et al. IL-31 plays dual roles in lung inflammation in an OVA-induced murine asthma model. *Biol Open.* 2019;8(1).
87. Flayer CH, Ge MQ, Hwang JW, et al. Ozone Inhalation Attenuated the Effects of Budesonide on Aspergillus fumigatus-Induced Airway Inflammation and Hyperreactivity in Mice. *Front Immunol.* 2019;10:2173.
88. Ravanetti L, Dijkhuis A, Dekker T, et al. IL-33 drives influenza-induced asthma exacerbations by halting innate and adaptive antiviral immunity. *The Journal of allergy and clinical immunology.* 2019;143(4):1355-1370 e1316.
89. Li R, Wang J, Zhu F, et al. HMGB1 regulates T helper 2 and T helper17 cell differentiation both directly and indirectly in asthmatic mice. *Molecular immunology.* 2018;97:45-55.
90. Fribley A, Zhang K, Kaufman RJ. Regulation of apoptosis by the unfolded protein response. *Methods Mol Biol.* 2009;559:191-204.
91. Pathinayake PS, Hsu AC, Waters DW, Hansbro PM, Wood LG, Wark PAB. Understanding the Unfolded Protein Response in the Pathogenesis of Asthma. *Front Immunol.* 2018;9:175.
92. Yaghi A, Dolovich MB. Airway Epithelial Cell Cilia and Obstructive Lung Disease. *Cells.* 2016;5(4).
93. Thomas B, Rutman A, Hirst RA, et al. Ciliary dysfunction and ultrastructural abnormalities are features of severe asthma. *The Journal of allergy and clinical immunology.* 2010;126(4):722-729 e722.
94. Aizawa H, Koarai A, Shishikura Y, et al. Oxidative stress enhances the expression of IL-33 in human airway epithelial cells. *Respir Res.* 2018;19(1):52.
95. Golebski K, Luiten S, van Egmond D, et al. High degree of overlap between responses to a virus and to the house dust mite allergen in airway epithelial cells. *PloS one.* 2014;9(2):e87768.
96. Liu B, Sun H, Wang J, Liu H, Zhao C. Potential role for EZH2 in promotion of asthma through suppression of miR-34b transcription by inhibition of FOXO3. *Lab Invest.* 2021;101(8):998-1010.
97. Barnes PJ, Adcock IM. Transcription factors and asthma. *Eur Respir J.* 1998;12(1):221-234.
98. Caramori G, Casolari P, Adcock I. Role of transcription factors in the pathogenesis of asthma and COPD. *Cell Commun Adhes.* 2013;20(1-2):21-40.
99. Sun Z, Xu X, He J, et al. EGR1 recruits TET1 to shape the brain methylome during development and upon neuronal activity. *Nat Commun.* 2019;10(1):3892.
100. Yang YA, Zhao JC, Fong KW, et al. FOXA1 potentiates lineage-specific enhancer activation through modulating TET1 expression and function. *Nucleic acids research.* 2016;44(17):8153-8164.

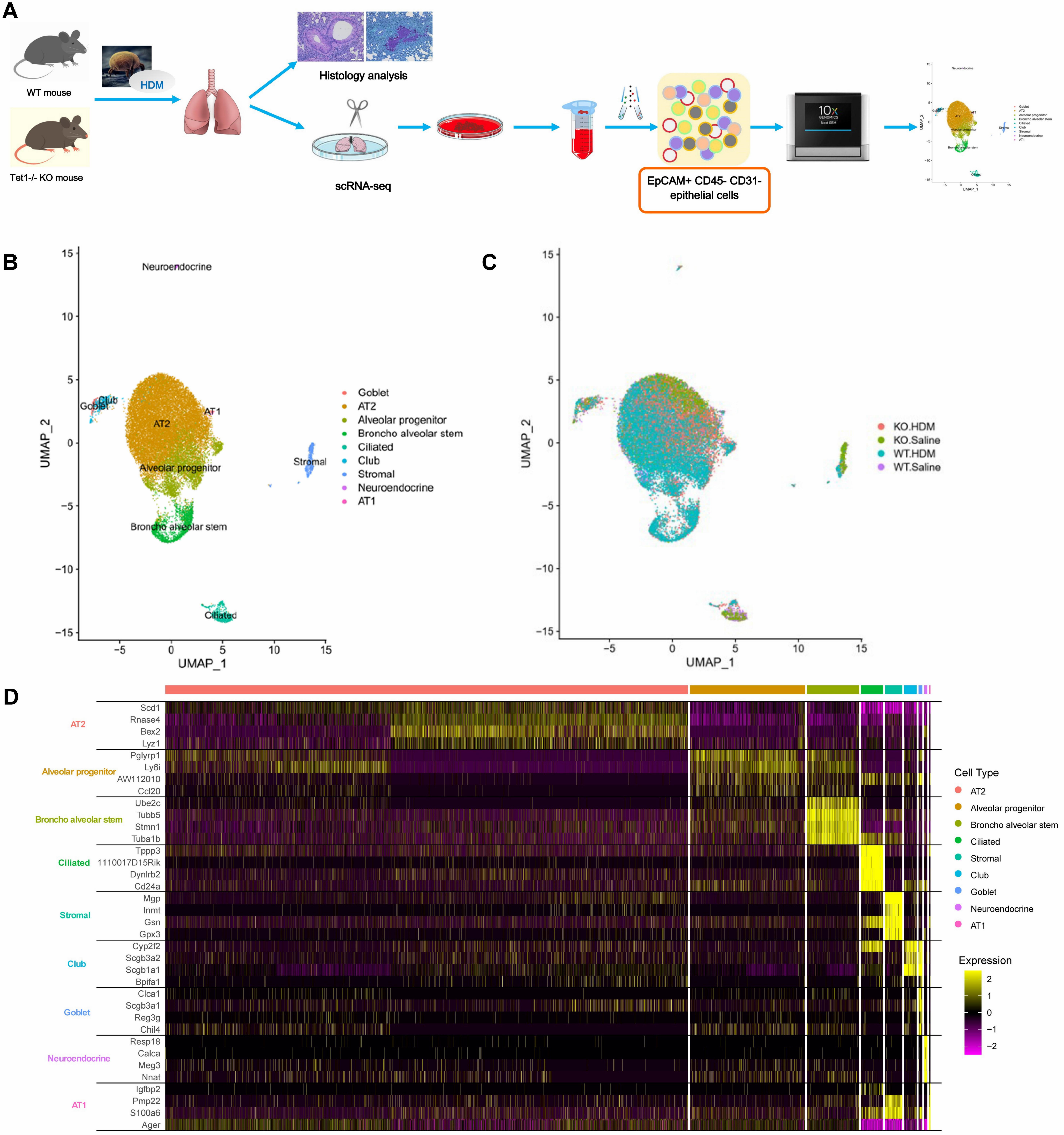
A
WT mouse
Tet1-/- KO mouse
HDM
Histology analysis
scRNA-seq
EpCAM+ CD45- CD31- epithelial cells
10x GENOMICS Next GEM
B
Neuroendocrine
Goblet
Club
AT2
AT1
Alveolar progenitor
Stromal
Broncho alveolar stem
Ciliated
UMAP_2
UMAP_1
15
10
5
0
−5
−10
−15
−5
0
5
10
15
Goblet
AT2
Alveolar progenitor
Broncho alveolar stem
Ciliated
Club
Stromal
Neuroendocrine
AT1
C
KO.HDM
KO.Saline
WT.HDM
WT.Saline
UMAP_2
UMAP_1
D
AT2
Scd1
Rnase4
Bex2
Lyz1
Alveolar progenitor
Pglyrp1
Ly6i
AW112010
Ccl20
Broncho alveolar stem
Ube2c
Tubb5
Stmn1
Tuba1b
Ciliated
Tppp3
1110017D15Rik
Dynlrb2
Cd24a
Stromal
Mgp
Inmt
Gsn
Gpx3
Club
Cyp2f2
Scgb3a2
Scgb1a1
Bpifa1
Goblet
Clca1
Scgb3a1
Reg3g
Chil4
Neuroendocrine
Resp18
Calca
Meg3
Nnat
AT1
Igfbp2
Pmp22
S100a6
Ager
Cell Type
AT2
Alveolar progenitor
Broncho alveolar stem
Ciliated
Stromal
Club
Goblet
Neuroendocrine
AT1
Expression
2
1
0
−1
−2

A
8000
7000
6000
5000
4000
3000
2000
1000
0
Cell count
WT-Sal
WT-HDM
KO-Sal
KO-HDM
AT1
AT2
Alveolar progenitor
Broncho alveolar stem
Ciliated
Club
Goblet
Neuroendocrine
B
100%
90%
80%
70%
60%
50%
40%
30%
20%
10%
0%
Cell percentage
WT-Sal
WT-HDM
KO-Sal
KO-HDM
AT1
AT2
Alveolar progenitor
Broncho alveolar stem
Ciliated
Club
Goblet
Neuroendocrine

A
WT HDM vs WT Sal DE genes
Intersection size
0
100
200
300
321
219
105
68
63
49
26
25
18
17
16
15
11
11
10
6
5
4
4
3
3
3
2
2
2
2
2
2
AT2
Alveolar progenitor
Ciliated
Broncho alveolar stem
Neuroendocrine
Club
Goblet
0
200
400
600
Set size
B
KO Sal vs WT Sal DE genes
Intersection size
0
20
40
49
22
13
11
3
2
2
1
1
1
1
1
1
1
AT2
Ciliated
Alveolar progenitor
Club
Broncho alveolar stem
Neuroendocrine
0
20
40
60
Set size
C
KO HDM vs WT Sal DE genes
Intersection size
0
100
200
300
332
217
87
82
40
27
26
25
20
15
14
14
12
10
8
7
7
5
5
4
4
3
3
2
2
2
AT2
Alveolar progenitor
Ciliated
Broncho alveolar stem
Club
Neuroendocrine
AT1
0
200
400
600
Set size
D
KO HDM vs WT HDM DE genes
Intersection size
0
10
20
30
32
25
16
10
8
5
5
AT2
Alveolar progenitor
Broncho alveolar stem
0
20
40
60
80
Set size

All EpCAM+ cells

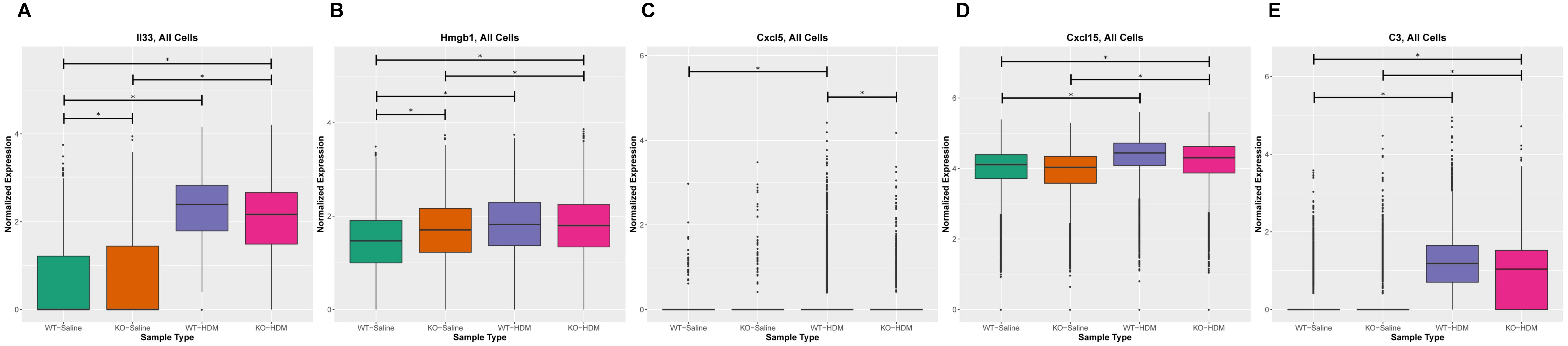

AT2 cells

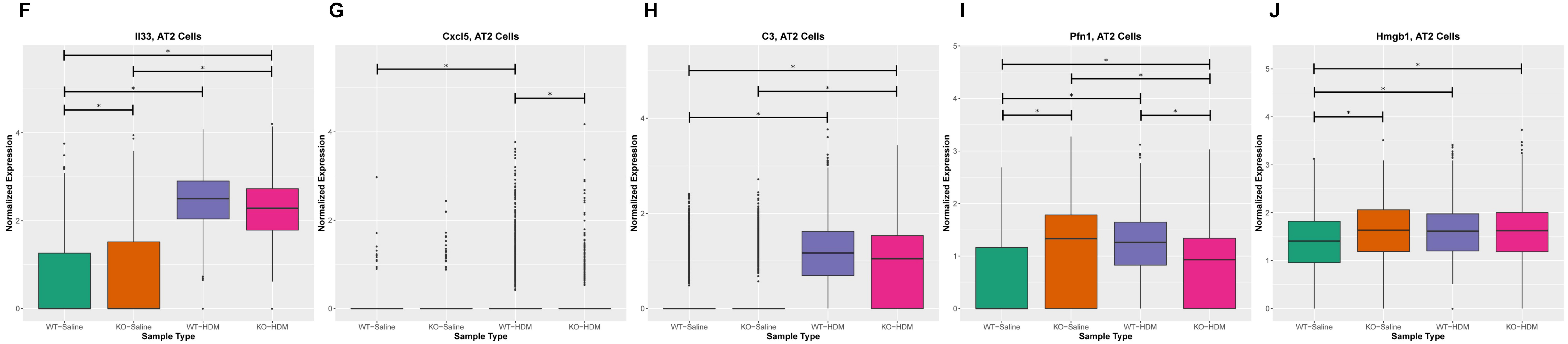

Ciliated cells

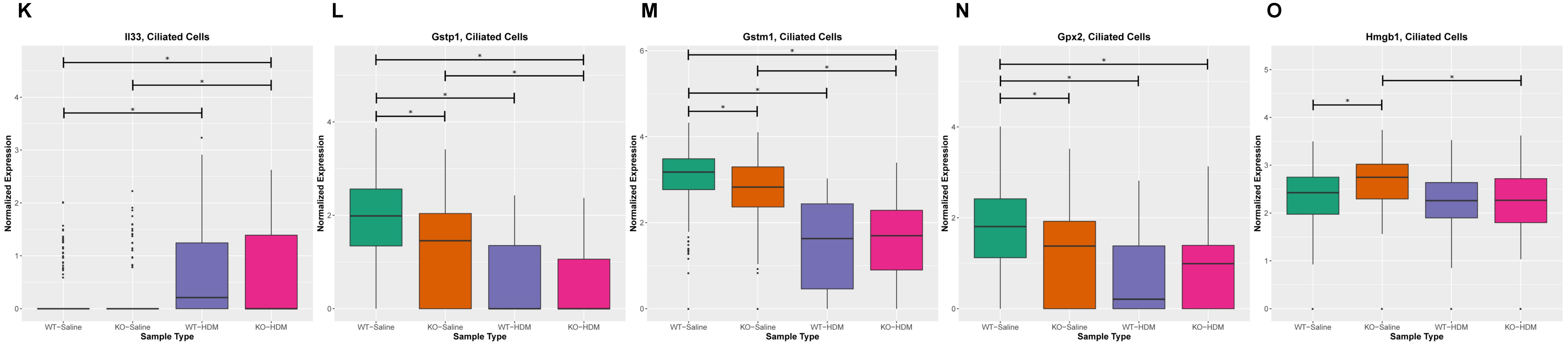

All EpCAM+ cells

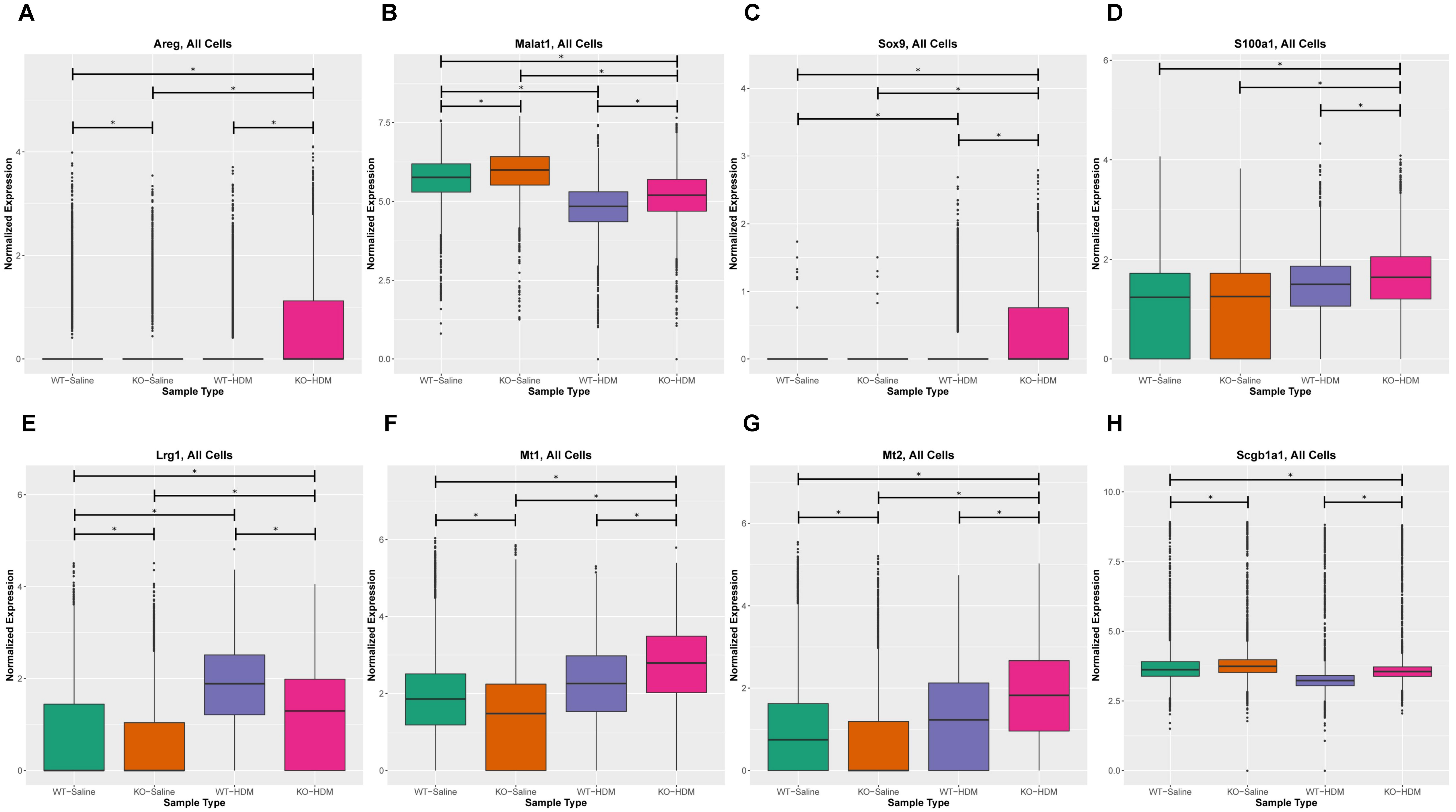

AT2 cells

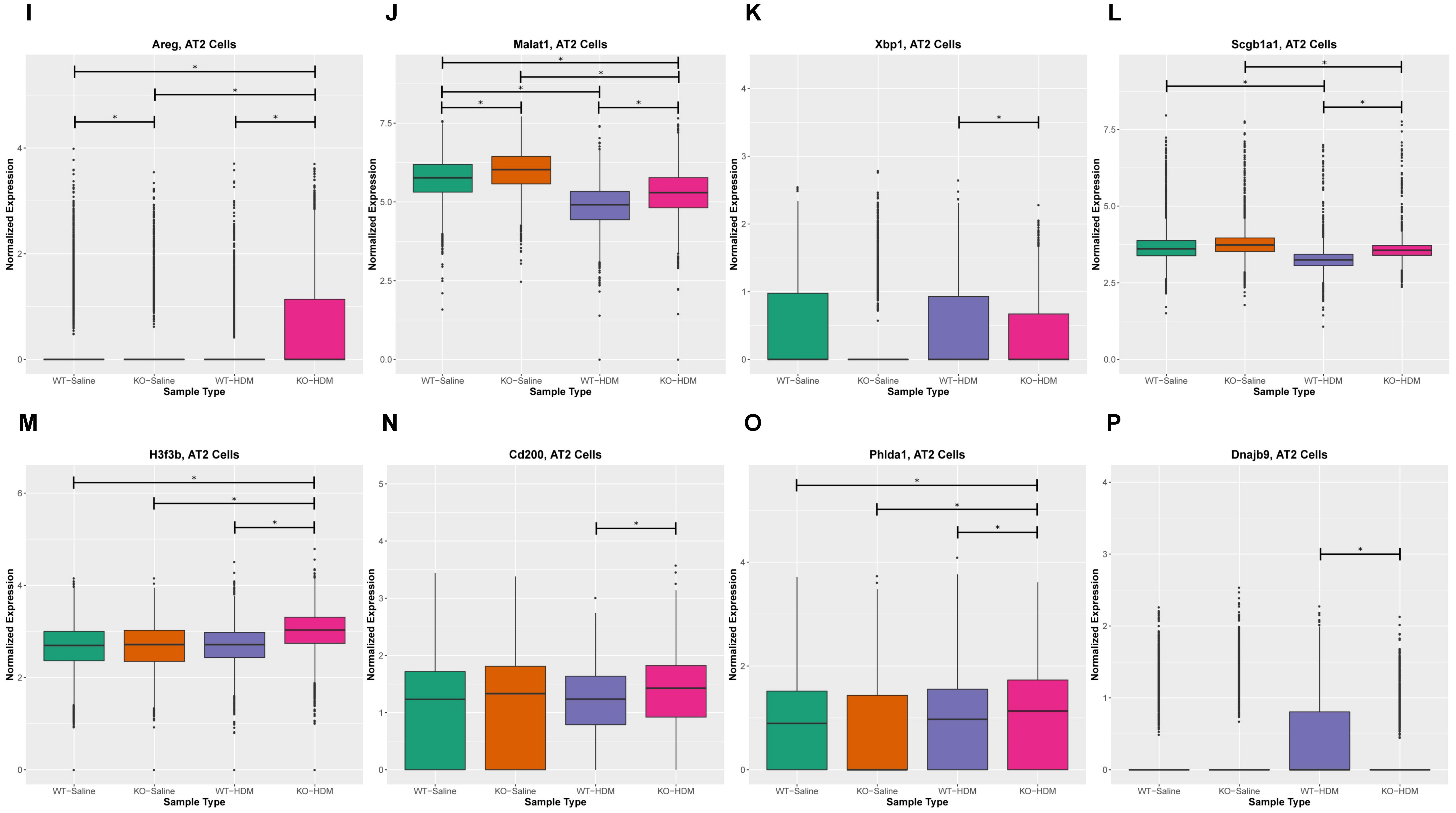

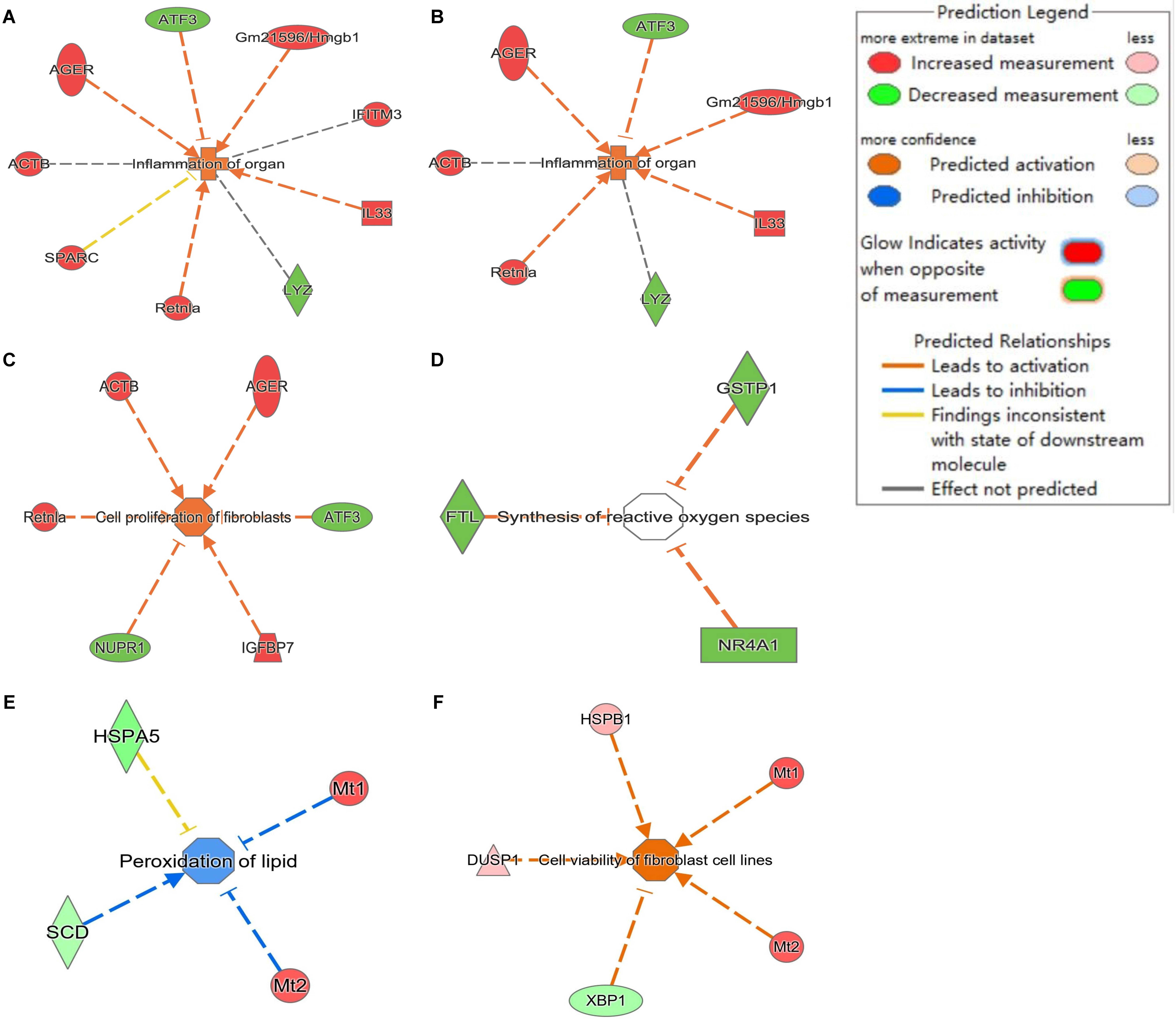
A
ATF3
Gm21596/Hmgb1
AGER
IFITM3
ACTB
Inflammation of organ
IL33
SPARC
LYZ
Retnla
B
ATF3
AGER
Gm21596/Hmgb1
ACTB
Inflammation of organ
IL33
Retnla
LYZ
Prediction Legend
more extreme in dataset
less
Increased measurement
Decreased measurement
more confidence
less
Predicted activation
Predicted inhibition
Glow Indicates activity when opposite of measurement
Predicted Relationships
Leads to activation
Leads to inhibition
Findings inconsistent with state of downstream molecule
Effect not predicted
C
ACTB
AGER
Retnla
Cell proliferation of fibroblasts
ATF3
NUPR1
IGFBP7
D
GSTP1
FTL
Synthesis of reactive oxygen species
NR4A1
E
HSPA5
Mt1
Peroxidation of lipid
SCD
Mt2
F
HSPB1
Mt1
DUSP1
Cell viability of fibroblast cell lines
Mt2
XBP1

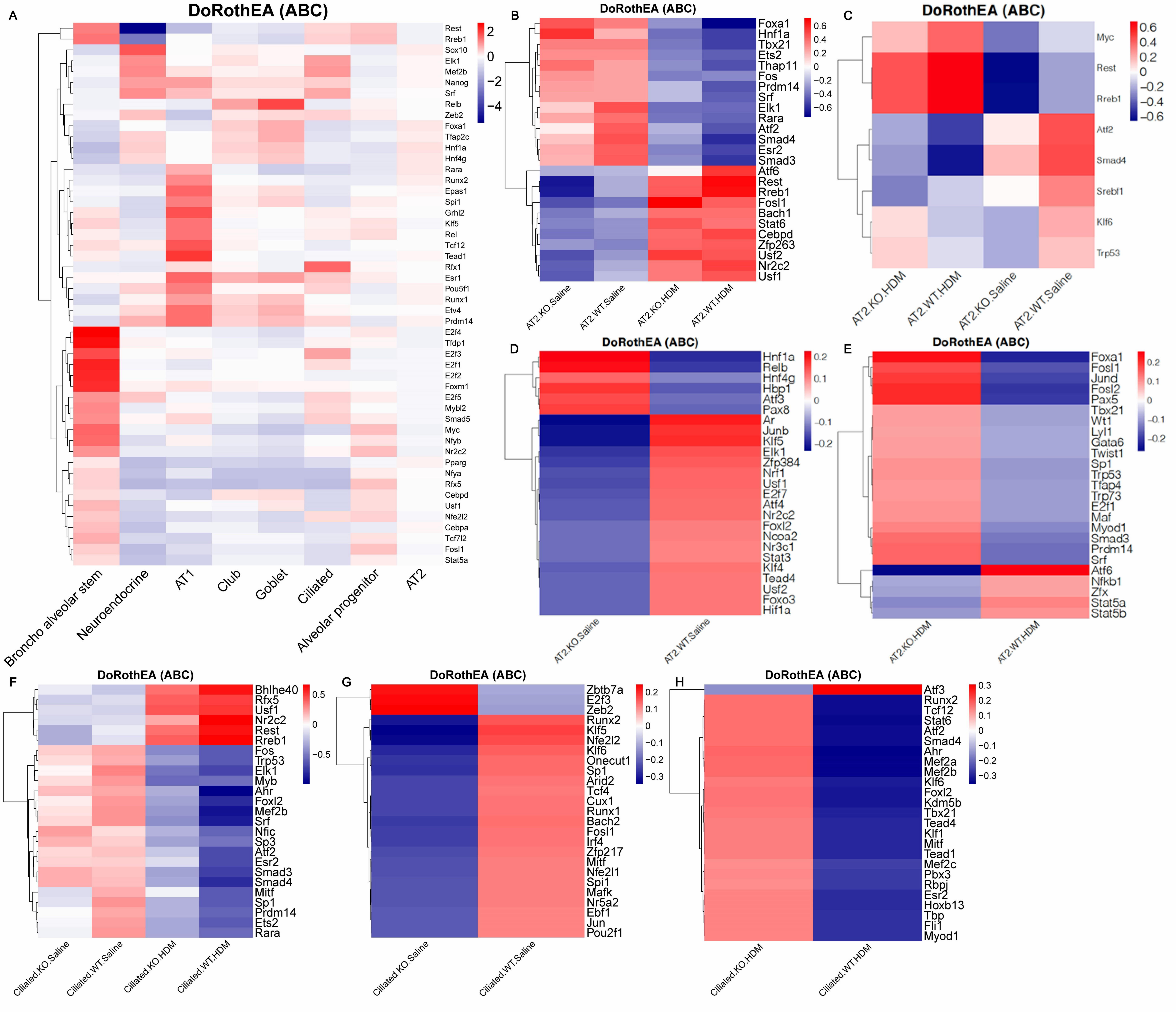A
DoRothEA (ABC)
Rest
Rreb1
Sox10
Elk1
Mef2b
Nanog
Srf
Relb
Zeb2
Foxa1
Tfap2c
Hnf1a
Hnf4g
Rara
Runx2
Epas1
Spi1
Grhl2
Klf5
Rel
Tcf12
Tead1
Rfx1
Esr1
Pou5f1
Runx1
Etv4
Prdm14
E2f4
Tfdp1
E2f3
E2f1
E2f2
Foxm1
E2f5
Mybl2
Smad5
Myc
Nfyb
Nr2c2
Pparg
Nfya
Rfx5
Cebpd
Usf1
Nfe2l2
Cebpa
Tcf7l2
Fosl1
Stat5a
2
0
−2
−4
Broncho alveolar stem
Neuroendocrine
AT1
Club
Goblet
Ciliated
Alveolar progenitor
AT2
B
DoRothEA (ABC)
Foxa1
Hnf1a
Tbx21
Ets2
Thap11
Fos
Prdm14
Srf
Elk1
Rara
Atf2
Smad4
Esr2
Smad3
Atf6
Rest
Rreb1
Fosl1
Bach1
Stat6
Cebpd
Zfp263
Usf2
Nr2c2
Usf1
0.6
0.4
0.2
0
−0.2
−0.4
−0.6
AT2.KO.Saline
AT2.WT.Saline
AT2.KO.HDM
AT2.WT.HDM
C
DoRothEA (ABC)
Myc
Rest
Rreb1
Atf2
Smad4
Srebf1
Klf6
Trp53
0.6
0.4
0.2
0
−0.2
−0.4
−0.6
AT2.KO.HDM
AT2.WT.HDM
AT2.KO.Saline
AT2.WT.Saline
D
DoRothEA (ABC)
Hnf1a
Relb
Hnf4g
Hbp1
Atf3
Pax8
Ar
Junb
Klf5
Elk1
Zfp384
Nrf1
Usf1
E2f7
Atf4
Nr2c2
Foxl2
Ncoa2
Nr3c1
Stat3
Klf4
Tead4
Usf2
Foxo3
Hif1a
0.2
0.1
0
−0.1
−0.2
AT2.KO.Saline
AT2.WT.Saline
E
DoRothEA (ABC)
Foxa1
Fosl1
Jund
Fosl2
Pax5
Tbx21
Wt1
Lyl1
Gata6
Twist1
Sp1
Trp53
Tfap4
Trp73
E2f1
Maf
Myod1
Smad3
Prdm14
Srf
Atf6
Nfkb1
Zfx
Stat5a
Stat5b
0.2
0.1
0
−0.1
−0.2
AT2.KO.HDM
AT2.WT.HDM
F
DoRothEA (ABC)
Bhlhe40
Rfx5
Usf1
Nr2c2
Rest
Rreb1
Fos
Trp53
Elk1
Myb
Ahr
Foxl2
Mef2b
Srf
Nfic
Sp3
Atf2
Esr2
Smad3
Smad4
Mitf
Sp1
Prdm14
Ets2
Rara
0.5
0
−0.5
Ciliated.KO.Saline
Ciliated.WT.Saline
Ciliated.KO.HDM
Ciliated.WT.HDM
G
DoRothEA (ABC)
Zbtb7a
E2f3
Zeb2
Runx2
Klf5
Nfe2l2
Klf6
Onecut1
Sp1
Arid2
Tcf4
Cux1
Runx1
Bach2
Fosl1
Irf4
Zfp217
Mitf
Nfe2l1
Spi1
Mafk
Nr5a2
Ebf1
Jun
Pou2f1
0.2
0.1
0
−0.1
−0.2
−0.3
Ciliated.KO.Saline
Ciliated.WT.Saline
H
DoRothEA (ABC)
Atf3
Runx2
Tcf12
Stat6
Atf2
Smad4
Ahr
Mef2a
Mef2b
Klf6
Foxl2
Kdm5b
Tbx21
Tead4
Klf1
Mitf
Tead1
Mef2c
Pbx3
Rbpj
Esr2
Hoxb13
Tbp
Fli1
Myod1
0.3
0.2
0.1
0
−0.1
−0.2
−0.3
Ciliated.KO.HDM
Ciliated.WT.HDM

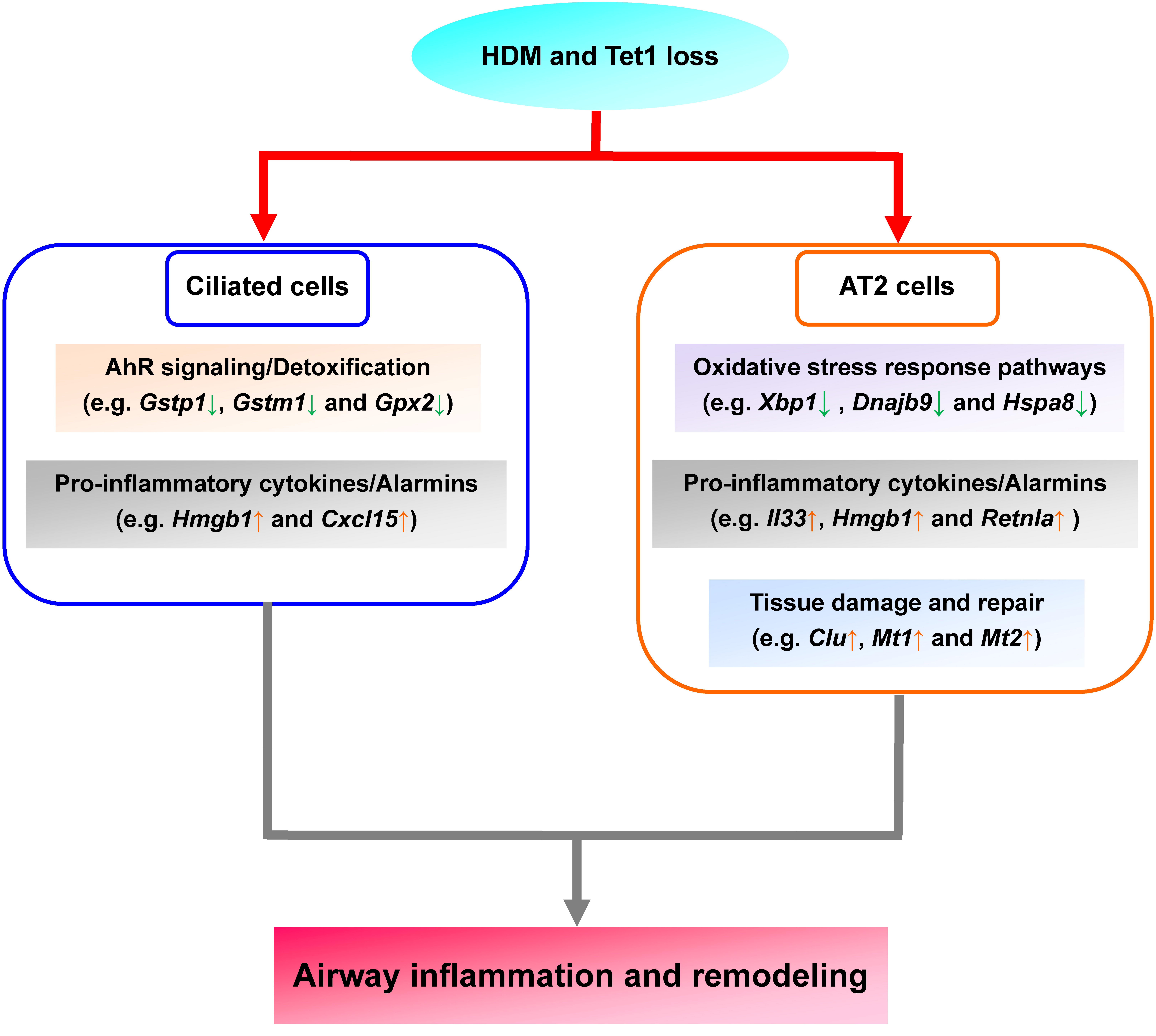
HDM and Tet1 loss
Ciliated cells
AhR signaling/Detoxification
(e.g. *Gstp1*↓, *Gstm1*↓ and *Gpx2*↓)
Pro-inflammatory cytokines/Alarmins
(e.g. *Hmgb1*↑ and *Cxcl15*↑)
AT2 cells
Oxidative stress response pathways
(e.g. *Xbp1*↓ , *Dnajb9*↓ and *Hspa8*↓)
Pro-inflammatory cytokines/Alarmins
(e.g. *Il33*↑, *Hmgb1*↑ and *Retnla*↑)
Tissue damage and repair
(e.g. *Clu*↑, *Mt1*↑ and *Mt2*↑)
Airway inflammation and remodeling